(2)

TECHNICAL REPORT BRL-TR-3385

BRL

DETERMINATION OF OPERABLE DEFORMATION MECHANISMS DURING BALLISTIC IMPACT IN TUNGSTEN SINGLE CRYSTALS, UTILIZING TRANSMISSION ELECTRON MICROSCOPY

R. A. HERRING

AUGUST 1992

U.S. ARMY LABORATORY COMMAND

BALLISTIC RESEARCH LABORATORY
ABERDEEN PROVING GROUND, MARYLAND

NOTICES

Destroy this report when it is no longer needed. DO NOT return it to the originator.

Additional copies of this report may be obtained from the National Technical Information Service, U.S. Department of Commerce, 5285 Port Royal Road, Springfield, VA 22161.

The findings of this report are not to be construed as an official Department of the Army position, unless so designated by other authorized documents.

The use of trade names or manufacturers' names in this report does not constitute indorsement of any commercial product.

REPORT DOCUMENTATION PAGE

Form Approved
OMB No. 0704-0188

1. AGENCY USE ONLY (Leave blank)	2. REPORT DATE	3. REPORT TYPE AND DATES COVERED
	August 1992	Final, 30 March 91 - 15 May 91

4. TITLE AND SUBTITLE
Determination of Operable Deformation Mechanisms During Ballistic Impact in Tungsten Single Crystals, Utilizing Transmission Electron Microscopy

5. FUNDING NUMBERS
44592-102-09-6704
CC 446700

6. AUTHOR(S)
R. A. Herring

7. PERFORMING ORGANIZATION NAME(S) AND ADDRESS(ES)

8. PERFORMING ORGANIZATION REPORT NUMBER

9. SPONSORING / MONITORING AGENCY NAME(S) AND ADDRESS(ES)
U.S. Army Ballistic Research Laboratory
ATTN: SLCBR-DD-T
Aberdeen Proving Ground, MD 21005-5066

10. SPONSORING / MONITORING AGENCY REPORT NUMBER
BRL-TR-3385

11. SUPPLEMENTARY NOTES

12a. DISTRIBUTION / AVAILABILITY STATEMENT
Approved for public release; distribution is unlimited.

12b. DISTRIBUTION CODE

13. ABSTRACT (Maximum 200 words)

The performance of tungsten single crystals in ballistic impact varies strongly as a function of crystallographic orientation. The deformation structure of recovered single crystal rods fired in ballistic environments has been characterized by optical microscopy, SEM and TEM, and x-ray diffraction. The observed microstructures are varied and provide substantial insights into the factors governing the penetration and flow behavior under ballistic conditions. Crystallographic orientation influences the potential for developing shear which enhances material flow, and this enhancement ultimately maximizes the energy available for target penetration. Microstructural analysis elucidates the various mechanisms occurring during the flow process for single crystals of high-symmetry orientations, and suggests possible analogies between the penetration behavior of the tungsten single crystals and other materials.

14. SUBJECT TERMS
tungsten; ballistics; transmission electron microscopy; dislocations

15. NUMBER OF PAGES
55

16. PRICE CODE

17. SECURITY CLASSIFICATION OF REPORT	18. SECURITY CLASSIFICATION OF THIS PAGE	19. SECURITY CLASSIFICATION OF ABSTRACT	20. LIMITATION OF ABSTRACT
UNCLASSIFIED	UNCLASSIFIED	UNCLASSIFIED	UL

INTENTIONALLY LEFT BLANK.

TABLE OF CONTENTS

		Page
	LIST OF FIGURES	v
	LIST OF TABLES	ix
	ACKNOWLEDGMENTS	xi
1.	INTRODUCTION	1
2.	METHODS	1
2.1	Transmission Electron Microscopy	1
2.2	Specimen Preparation	3
3.	RESULTS	3
3.1	[100]-Oriented Penetrator	5
3.2	[110]-Oriented Penetrator	5
3.3	[111]-Oriented Penetrator	15
4.	DISCUSSION	23
4.1	Analysis of Dislocations at Subgrain Boundaries	26
4.2	General Microscopic Deformation	26
4.3	Recrystallization	30
4.4	Macrodeformation of Penetrators and Mass Flow	30
4.5	Ability of Penetrator to Penetrate RHA Shielding Material	36
5.	REFERENCES	37
	DISTRIBUTION LIST	39

INTENTIONALLY LEFT BLANK.

LIST OF FIGURES

Figure		Page
1.	Deformation of the [100] Penetrator by a Disorderly Arrangement of Dislocations Which Have Burgers Vectors of 1/2<111> Showing a) the Initial Stages of Subgrain Formation, b) the Initial Formation of Well-Defined Individual Grains, c) the Elongation of Grains, and d) the Formation of Well-Defined Elongated Grains	4
2.	Recrystallized Regions Which Show Well-Defined Grains of Different Orientation (Large Variation in Light/Dark Contrast), With Little or No Dislocations Within the Grains	6
3.	The Analysis of a Dislocation Network of a Region Close to That Shown in Figure 1a From a [100] Penetrator Showing Many Two-Beam Electron Diffraction Conditions Which Put the Dislocations, Which Are Labelled A, B, C, and D, In or Out of Contrast. For Illustration the Micrographs of a) and c), as Well as b) and d), Show +g Diffraction Vectors. In Addition, the Micrographs of d) and f) Show How the Contrast of the Dislocations Change With the Deviation From the Exact Bragg Diffraction With f) Being Closer to the Exact Bragg Condition. Please See the Text, Figure 4, Table 1, and Table 2 for Further Information	7
4a.	Stereograms of the *[100] Projection Showing the Intersection of Three* Projected Planes at the [1$\bar{1}$1] Zone Axis, Which Were Taken From the Projected Line Directions at Their Respective Beam Directions of the Dislocations Which Are Labelled A in Figure 3. These Dislocations Have a Burgers Vector of 1/2 [1$\bar{1}$1] and Have a Line Direction of [1$\bar{1}$1] and Thus Are Pure Screw Dislocations	10
4b.	Stereograms of the [100] Projection Showing the Intersection of Four Projected Planes Between the [012] and the [111] Zone Axis, Which Were Taken From the Projected Line Directions at Their Respective Beam Directions of the Dislocations Which Are Labelled B in Figure 3. These Dislocations Have a Burgers Vector of 1/2 [111] and Have a Line Direction Between [111] and [012] Which Makes Them Pure Screw Dislocations or They Have a Large Screw Component and Lie on the (1$\bar{2}$1)	11
4c.	Stereograms of the [100] Projection Showing the Intersection of Three Projected Planes Around the [$\bar{1}$11] Zone Axis, Which Were Taken From the Projected Line Directions at Their Respective Beam Directions of the Dislocations Which Are Labelled C in Figure 3. These Dislocations Have a Burgers Vector of 1/2 [$\bar{1}$11] and Have a Line Direction of [$\bar{1}$12] and Thus Lie on the (110)	12

Figure — Page

4d. Stereograms of the [100] Projection Showing the Intersection of Three Projected Planes Between the [$\bar{1}\bar{1}2$], [$\bar{1}02$], and the [$\bar{1}\bar{1}1$] Zone Axis, Which Were Taken From the Projected Line Directions at Their Respective Beam Directions of the Dislocations Which Are Labelled D in Figure 3. These Dislocations Had a Burgers Vector of 1/2 [$\bar{1}\bar{1}1$] and Thus Have a Large Screw Component 13

5. The General Microstructure of the Deformed [110] Penetrator Showing a) to c) Heavily Dislocated, Well-Defined, Elongated Grains and d) Some Recrystallization Which Has Produced Small Grains of Low Dislocation Density. 14

6. The Analysis of a Dislocation Network of a Region Close to Those Shown in Figure 5 From a [110] Penetrator Showing Many Two-Beam Electron Diffraction Conditions Which Put the Dislocations, Which Are Labelled A, B, and C, In or Out of Contrast. Note That c) Clearly Shows Segments of Dislocation Which Have Edge Character (Labelled by Arrows). Please See the Text and Table 3 and Table 4 for Further Information 16

7a. Stereograms of the [110] Projection Showing the Intersection of Five Projected Planes Close to the [11$\bar{1}$] Zone Axis, Which Were Taken From the Projected Line Direction at Their Respective Beam Directions of the Dislocations Which Are Labelled A in Figure 6. These Dislocations Had a Burgers Vector of 1/2 [11$\bar{1}$] and Thus Have a Large Screw Component ... 19

7b. Stereograms of the [110] Projection Showing the Intersection of Three Projected Planes Close to the [1$\bar{1}$1] Zone Axis, Which Were Taken From the Projected Line Directions at Their Respective Beam Directions of the Dislocations Which Are Labelled A in Figure 6. These Dislocations Had a Burgers Vector of 1/2 [1$\bar{1}$1] and Thus Have a Large Screw Component 20

8. The General Microstructure of the Deformed [111] Penetrator Showing an Orderly Arrangement of Dislocations Which Have Formed a High Density of Dislocations at the Subgrain Boundaries 21

9. The Analysis of a Dislocation Network From a [111] Penetrator Showing Many Two-Beam Electron Diffraction Conditions Which Put the Dislocations, Which Are Labelled A, B, and C, In or Out of Contrast. A Two-Beam Electron Diffraction Pattern Is Shown in f). Please See the Text and Table 5 and Table 6 for Further Information 22

10a. Stereograms of the [111] Projection Showing the Intersection of Three Projected Planes Close to the [111] Zone Axis, Which Were Taken From the Projected Line Directions at Their Respective Beam Directions of the Dislocations Which Are Labelled A in Figure 9. These Dislocations Had a Burgers Vector of 1/2 [111] and Thus Have a Large Screw Component 24

Figure | Page

10b. Stereograms of the [111] Projection Showing the Intersection of Three Projected Planes Close to the [11$\bar{1}$] Zone Axis, Which Were Taken From the Projected Line Directions at Their Respective Beam Directions of the Dislocations Which Are Labelled B in Figure 9. These Dislocations Had a Burgers Vector of 1/2 [11$\bar{1}$] and Thus Have a Large Screw Component . . . 25

11. A Square Crystal Deformed by (a) a Vertical Set of Screw Dislocations; (b) a Horizontal Set of Screw Dislocations; and (c) Both Sets of Screw Dislocations 29

12a. Residual Material From a [100]-Oriented Penetrator Fired Into RHA. Note the Formation of Slip Lines Which Are Similar to Those Seen in the [111] Penetrator (Figure 12c) at Around 55° to the Penetration Axis. See Text. 31

12b. Residual Material From a [110]-Oriented Penetrator Fired Into RHA. Note Reorientation of Residual Penetrator so That the [1$\bar{1}$0] Is Parallel to the Penetration Axis. See Text 32

12c. Residual Material From [111]-Oriented Penetrator Fired Into RHA. Note Slip Lines of Differently Oriented Layers of Material 33

13. Cottrell's Dislocation Intersection Mechanism to Explain {100} Crack Nuclei in b.c.c. Crystals Where a) Shows Two Dislocations Combining to Form a Crack Dislocation, b) the Additions of the Burgers Vectors, and c) the Orientation of the Crack 34

14. The Forcing Together of Edge-Type Dislocations of the Same Sign to Produce a Crack Nuclei 35

INTENTIONALLY LEFT BLANK.

LIST OF TABLES

Table		Page
1.	Analysis of Dislocation Contrast for Various Diffraction Vectors [100] Orientation, Specimen A1, Box 1, Film 980–1018	9
2.	Projected Line Direction for Various Dislocations With Respect to Diffraction Vectors [100] Orientation, Specimen A1, Box 1, Film 980–1018	9
3.	Analysis of Dislocation Contrast for Various Diffraction Vectors [110] Orientation, Specimen A1, Box 2, Film 1057–1102	18
4.	Projected Line Direction for Various Dislocations With Respect to Diffraction Vectors [110] Orientation, Specimen A1, Box 2, Film 1057–1102	18
5.	Analysis of Dislocation Contrast for Various Diffraction Vectors [111] Orientation, Specimen K1, Box 1, Film 452–463	23
6.	Projected Line Direction for Various Dislocations With Respect to Diffraction Vectors [111] Orientation, Specimen K1, Box 1, Film 452–463	23
7.	Critical Resolved Shear Stress Factors on Slip Planes for Various Orientation Penetrators	27

INTENTIONALLY LEFT BLANK.

ACKNOWLEDGMENTS

The author would like to thank Drs. Priscilla Kingman, William Bruchey, and Mr. Edward Horwath for their guidance and support during the duration of this project. The author's education and familiarity with the field of impact and penetration was greatly enhanced by the technical discussions with these individuals. Additionally, their help in preparing and having available the necessary facilities to conduct this study on-site at the U.S. Army Ballistic Research Laboratory (BRL), Aberdeen Proving Ground, MD was invaluable.

The author would also like to express his appreciation to Mr. David MacKenzie for his patience and expertise in preparing the transmission electron microscopy specimens.

INTENTIONALLY LEFT BLANK.

1. INTRODUCTION

The study of kinetic energy penetrator materials has generally been related to penetration depth into standard armor configurations and general "macro" views of penetrator target interactions. This approach has not led to a complete understanding of the mechanisms responsible for penetration performance of various kinetic energy penetrator materials. Recent studies (Gerlach 1986; Magness1990; Bruchey, Horwath, and Kingman 1991; and Stephens 1968) have shown that the penetrator is consumed by back-extruding from the penetrator/target interface, while the interface moves forward into the target. The penetrator material properties (i.e., density, mechanical properties, crystallography, etc.) have been shown to be very important materials parameters affecting ballistic performance.

The work presented in this report is a continuation of studies which were initiated by Bruchey, Horwath, and Kingman (1990, 1991), who were able to show significant differences in the high strain rate deformation behavior of tungsten single crystal penetrators having orientations of [100], [1$\bar{1}$0], and [111] when fired into rolled homogeneous armor (RHA).

The dislocation generation and interaction phenomena which allowed unique ballistic performance of each [100]-oriented, [110]-oriented, and [111]-oriented single-crystal rod are analyzed.

2. METHODS

A previous paper (Bruchey, Horwath, and Kingman 1990) presented initial light microscopy and macro SEM photos of the residual rod/target interface. This paper summarizes the results of an additional technique, Transmission Electron Microscopy (TEM). This technique allowed investigation of mechanisms responsible for ballistic behavior of each specific [110]-oriented, [111]-oriented, and [100]-oriented tungsten single-crystal penetrator.

2.1 Transmission Electron Microscopy. TEM was used to characterize the mechanism of deformation. The defects responsible for deformation, which consisted of dislocations, were characterized for their Burgers vector, $\underline{b}$, line direction, $\underline{u}$, and their habit planes, $\underline{R}$. The dislocations' habit plane contains both $\underline{b}$ and $\underline{u}$. The normal to this habit plane is given by

$\underline{R} = \underline{b} \times \underline{u}$. These parameters are necessary for the full characterization of edge and mixed (screw + edge components) dislocations. Screw dislocations which do not lie on habit planes have $\underline{b} = \underline{u}$. The characterization technique involved viewing the dislocations under many two-beam electron diffraction conditions.

The Burgers vector of a dislocation was determined by the $\underline{g}.\underline{b} = 0$ condition (i.e., zero contrast condition, where $\underline{g}$ is the electron diffraction vector) as well as by the contrast shown by the dislocations when $\underline{g}.\ \underline{b} = 1, 2$, or more.

Determining the dislocation line direction involved viewing the dislocation in more than one projection so the true direction could be extracted from the projected directions. A stereogram technique was often used to determine $\underline{u}$. The technique can be summarized as follows. In the case of a projected line direction [h, k, l] of a direction viewed in a direction B, all that can be said is that the true line direction lies in a plane defined by [h, k, l] and B1. Micrographs taken in any other beam direction B2 result in a second projected direction [h2, k2, l2] and hence a plane defined by [h2, k2, l2] and B2. The intersection of these two planes (i.e., the zone axis) defines the true line direction of the dislocation given by $\underline{u}$. When transferring the projected plane onto the stereogram, care must be taken to rotate the plane in the correct direction with respect to the diffraction vector and other directions on the stereogram. If the dislocation is bent or winding through the crystal, the line direction is often taken as a line which joins the beginning and end of the dislocation, or a general sense of direction is used. It should be mentioned that dislocations can only end at a free surface or another dislocation. The short segments of dislocations seen in the TEM are dislocations which are passing through the thin foil and intersecting both the top and bottom surfaces. For this reason, the true line direction of a dislocation could sometimes be determined by lining it up to produce a point rather than a line (i.e., the dislocation runs parallel to the beam direction).

When analyzing a region of a TEM specimen, an arbitrary crystal orientation is taken as a reference point, and any rotations are taken with respect to this point. It should be noted that it is difficult to know the exact crystallographic orientation of the TEM specimen with respect to the penetrator axis as the TEM specimen is small and is easily rotated and flipped over. Thus, the crystallographic relationships between penetrator orientation and TEM specimen

orientation must be inferred from the results and not directly from the crystallographic orientation of the TEM results.

2.2 Specimen Preparation. TEM specimens were prepared by slow speed diamond or graphite cutting of thin wafers (~0.5 mm) from the bulk W material. The wafers had 3-mm-diameter disks cut from them using a spark machine. The disks were lapped on SiC papers to a thickness of 50–100 μm using a parallel-sided grinding jig and grit size of 240 to 1,200. Final thinning involved electrochemical jet polishing in an aqueous 2% NaOH solution at 40 V until a hole perforated through the specimen, which produced electron transparent regions around the hole. Stephens (1968) had good success with making TEM W specimens using a similar method which involved electrochemical etching in a still bath of aqueous NaOH after first electrochemical jet etching to produce dimples in the specimens' surface.

Care was taken to cut the TEM specimen from specific regions of the penetrator and then to keep track of these specimens (with respect to their location) through the process of making TEM thin foils. However, the [110]-oriented specimens cracked upon spark-machine cutting so their location with respect to the penetrator was lost.

3. RESULTS

In the three types of penetrators (i.e., the single crystals of [100], [110], and [111]), certain microstructures were seen which could be generalized as follows. Dislocations were found with Burgers vectors of 1/2 <111>. No other type of defect which could produce deformation was found. The dislocations polyganized the crystal by forming grain boundaries. Recrystallization of the grains removed the dense dislocation networks and was seen in material which was on the order of hundreds of micrometers from regions which appeared to have been freshly deformed.

General views of the process by which the single-crystal penetrators are polygonized are shown in Figures 1a–1d, which were located at the penetrator/RHA interface of a [100]-oriented penetrator. The dislocations thread their way through the crystal and form dense arrays which are the basis for subgrain formation (Figure 1a). Well-defined grain boundaries have begun to form in Figure 1b, and eventually elongated grains form which have a high

Figure 1. Deformation of the [100] Penetrator by a Disorderly Arrangement of Dislocations Which Have Burgers Vectors of 1/2<111> Showing a) the Initial Stages of Subgrain Formation, b) the Initial Formation of Well-Defined Individual Grains, c) the Elongation of Grains, and d) the Formation of Well-Defined Elongated Grains.

density of dislocations within themselves (Figures 1c and 1d). Even though the deformation process followed this general pattern, the dislocation networks at the subgrain boundaries (and thus grain boundaries) were significantly different for each orientation, which was indicative of their different dislocation generation mechanisms.

General views of recrystallized regions are shown in Figures 2a–2d, which show grains of random orientation, well-defined grain boundaries, and a low dislocation network within the grains.

Results of the analysis of the deformation mechanism for the specific penetrator orientations are presented below, where a complete analysis of the dislocations are presented.

3.1 [100]-Oriented Penetrator. A complete analysis of a dislocation network, which was taken from a region close to that region shown in Figure 1a, is presented in Figures 3a–3j. Four types of dislocations which have been labelled A, B, C, and D dominate the microstructure. The dislocations labelled A and C tend to be somewhat straight, and those of B and D are wavey. All together they form a tangled, dense dislocation array. These dislocations are in and out of contrast for many diffraction vectors, and a summary is listed in Table 1. The dislocations which are labelled A, B, C, and D have a b = 1/2 $[1\bar{1}1]$, 1/2 [111], 1/2 $[\bar{1}11]$, and 1/2 $[11\bar{1}]$, respectively. The projected line directions of the dislocations labelled A, B, C, and D with respect to the diffraction vectors are listed in Table 2. The projected planes are plotted on the stereograms of Figures 4a–4d. The intersection of the projected planes, which give the true line direction u, can be seen to be very close to the direction of b and often occurred at one of the nearest <112> or <012> zone axis to b. Those dislocations which have u close to <112> reside on {110} habit planes, and those dislocations which have u close to <012> reside on {112} habit planes. Thus, the dislocations labelled A, B, C, and D are either pure screw dislocations or mixed dislocations with a large screw component.

3.2 [110]-Oriented Penetrator. General views of the deformation microstructure of a [110] penetrator (Figures 5a–5d) show elongated grains with a high density of dislocations, similar to that shown in Figure 1 for a [100] penetrator, except some regions appear to have small recrystallized grains (Figure 5d). A complete analysis of a dislocation network, which was

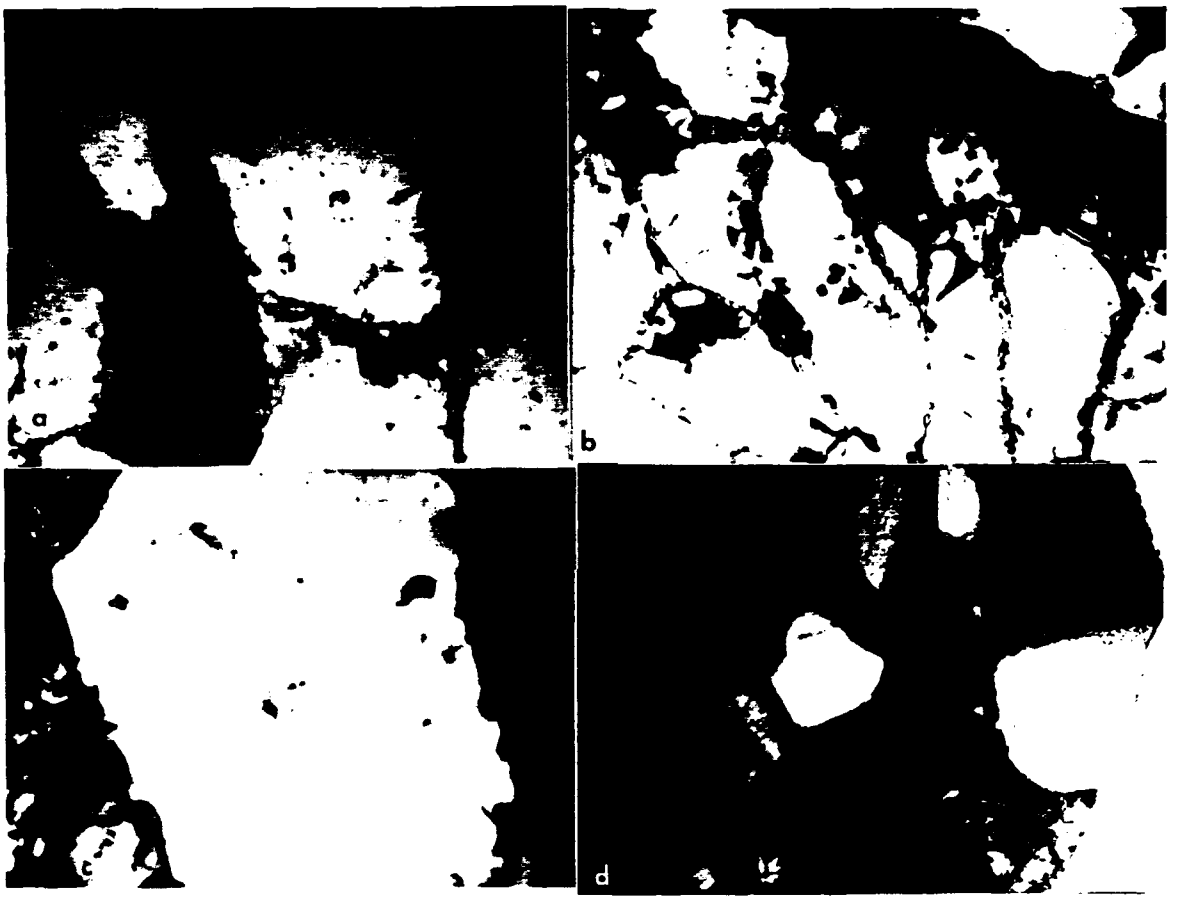

Figure 2. Recrystallized Regions Which Show Well-Defined Grains of Different Orientation (Large Variation in Light/Dark Contrast), With Little or No Dislocations Within the Grains.

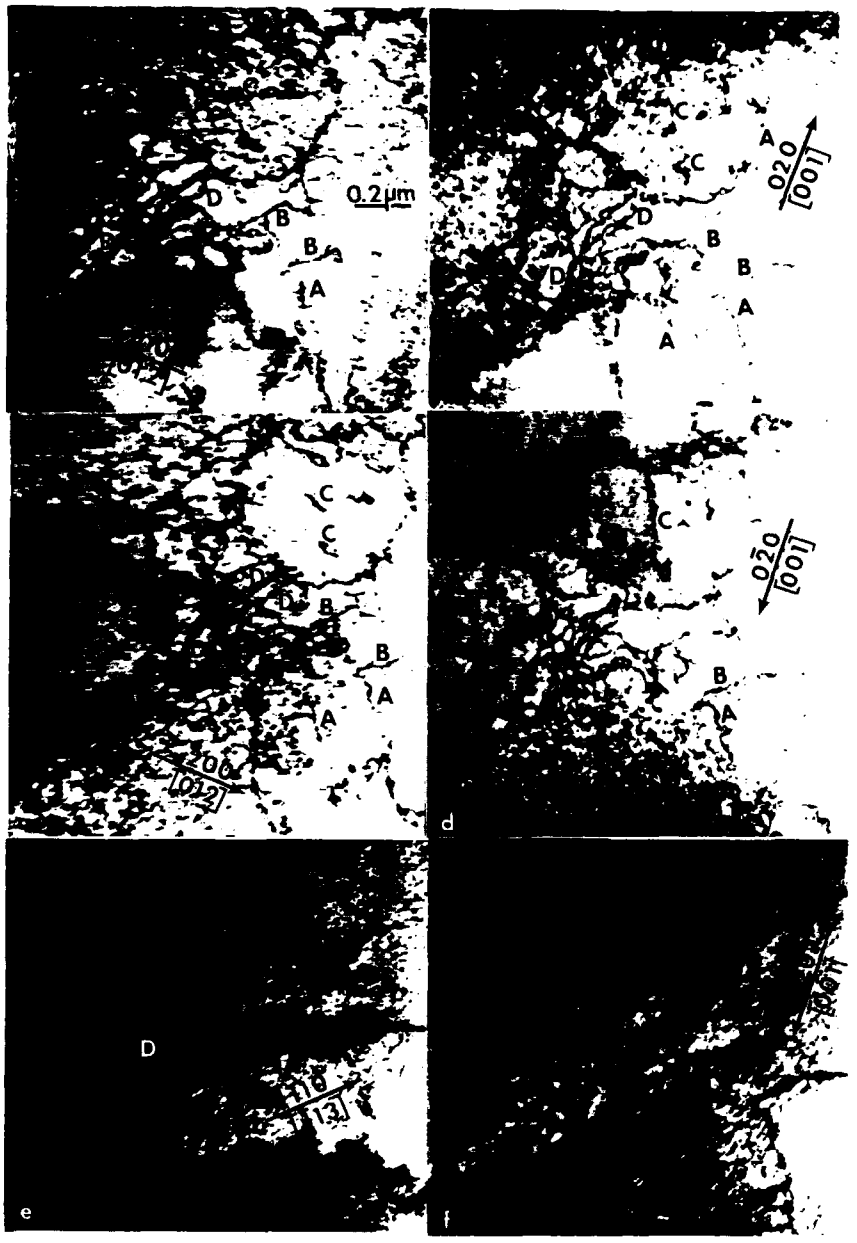

Figure 3. The Analysis of a Dislocation Network of a Region Close to That Shown in Figure 1a From a [100] Penetrator Showing Many Two-Beam Electron Diffraction Conditions Which Put the Dislocations, Which Are Labelled A, B, C, and D, In or Out of Contrast. For Illustration the Micrographs of a) and c), as Well as, b) and d) Show +g Diffraction Vectors. In Addition, the Micrographs of d) and f) Show How the Contrast of the Dislocations Change With the Deviation From the Exact Bragg Diffraction With f) Being Closer to the Exact Bragg Condition. Please See the Text, Figure 4, Table 1 and Table 2 for Further Information.

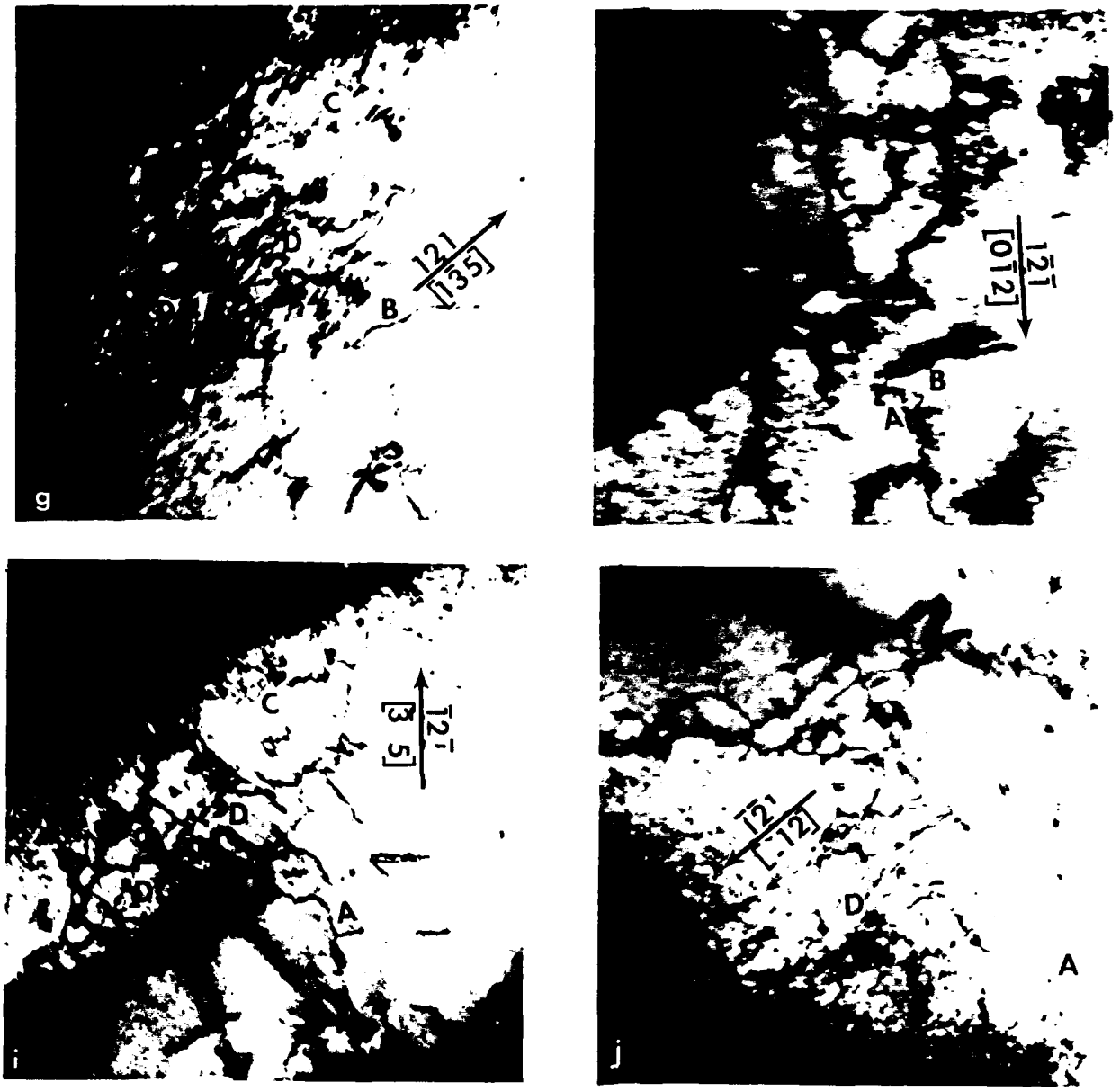

Figure 3. The Analysis of a Dislocation Network of a Region Close to That Shown in Figure 1a From a [100] Penetrator Showing Many Two-Beam Electron Diffraction Conditions Which Put the Dislocations, Which Are Labelled A, B, C, and D, In or Out of Contrast. For Illustration the Micrographs of a) and c), as Well as, b) and d) Show +g Diffraction Vectors. In Addition, the Micrographs of d) and f) Show How the Contrast of the Dislocations Change With the Deviation From the Exact Bragg Diffraction With f) Being Closer to the Exact Bragg Condition. Please See the Text, Figure 4, Table 1 and Table 2 for Further Information (Continued).

Table 1. Analysis of Dislocation Contrast for Various Diffraction Vectors
[100] Orientation, Specimen A1, Box 1, Film 980–1018

±g, Diffraction Vector [Zone Axis]	Dislocation Segments + in contrast, - out of contrast ? unsure of contrast			
	A	B	C	D
020 [001]	+	+	+	+
$1\bar{1}0$ [113]	+	-	+	-
$12\bar{1}$ [012]	+	+	-	+
200 [012]	+	+	+	+
$1\bar{2}1$ [$\bar{1}$13]	+	-	+	+
110 [$\bar{1}$13]	-	+	-	+
020 [001]	+	+	+	+
121 [0$\bar{1}$2]	-	+	+	+
$\bar{1}21$ [0$\bar{1}$2]	+	+	+	-
121 [1$\bar{3}$5]	-	+	+	+
$1\bar{2}1$ [$\bar{3}$15]	+	-	+	+
020 [001]	+	+	+	+
$2\bar{1}1$ [$\bar{1}$02]	+	+	+	-
2x<u>B</u>	<$1\bar{1}1$>	<111>	<$\bar{1}$11>	<$11\bar{1}$>

Table 2. Projected Line Direction for Various Dislocations With Respect to Diffraction Vectors
[100] Orientation, Specimen A1, Box 1, Film 980–1018

±g, Diffraction Vector [Zone Axis]	Dislocation Segments Angle of Rotation (°) cw clockwise ccw conterclockwise			
	A	B	C	D
020 [001]	–	–	52 ccw	–
$1\bar{1}0$ [113]	–	–	23 ccw	–
$12\bar{1}$ [012]	73 cw	20 cw	–	–
200 [012]	60 cw	42 cw	–	55 ccw
$1\bar{2}1$ [$\bar{1}$13]	–	–	–	–
110 [$\bar{1}$13]	–	–	–	20 ccw
020 [001]	–	–	–	–
121 [0$\bar{1}$2]	–	–	–	–
$\bar{1}21$ [0$\bar{1}$2]	–	72 cw	5 ccw	–
121 [1$\bar{3}$5]	–	10 cw	–	–
$1\bar{2}1$ [$\bar{3}$15]	–	–	–	45 cw
020 [001]	–	–	–	–
$2\bar{1}1$ [$\bar{1}$02]	53 ccw	–	–	–

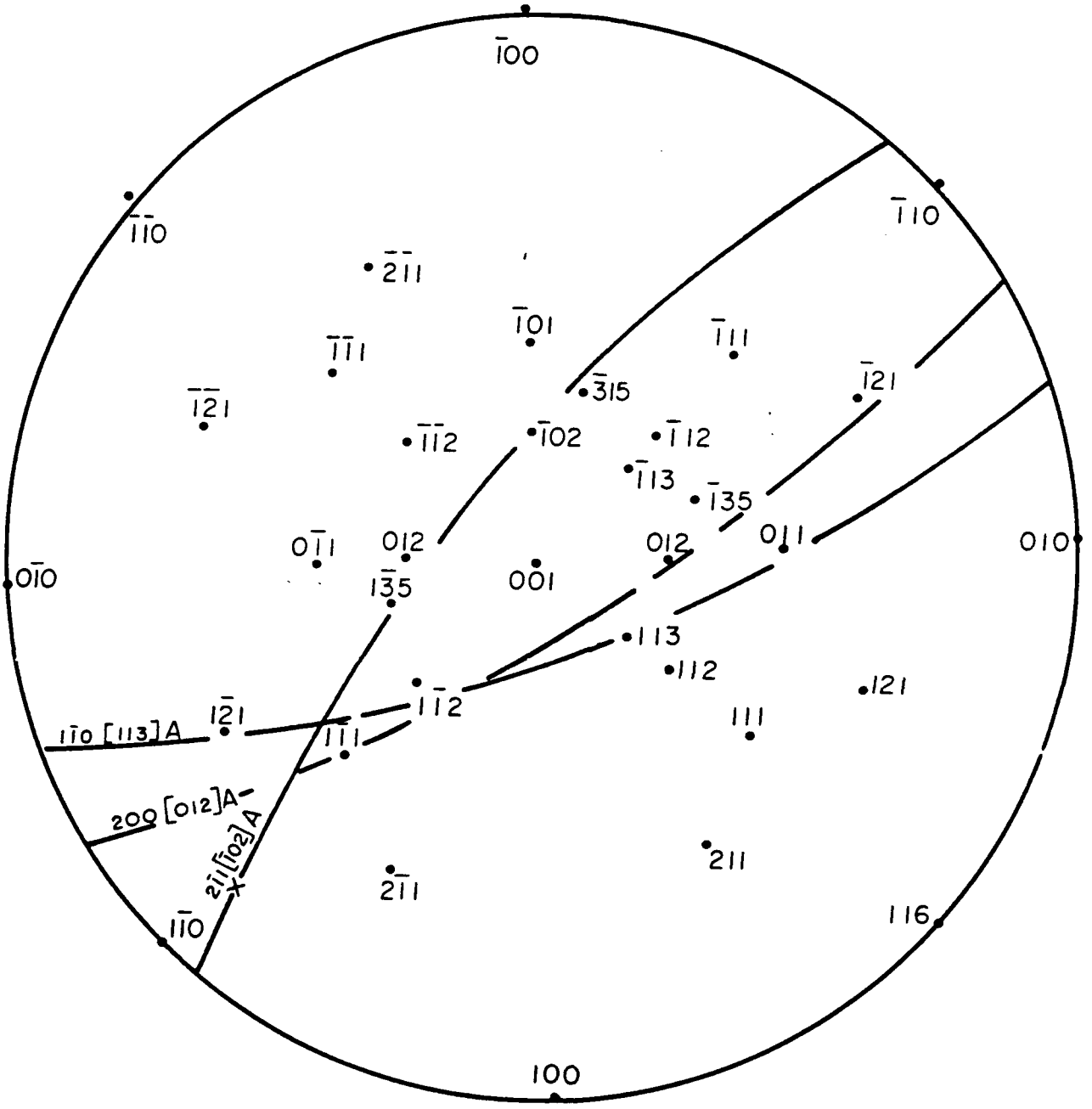

Figure 4a. Stereograms of the [100] Projection Showing the Intersection of Three Projected Planes at the [1$\bar{1}$1] Zone Axis, Which Were Taken From the Projected Line Directions at Their Respective Beam Directions of the Dislocations Which Are Labelled A in Figure 3. These Dislocations Have a Burgers Vector of 1/2 [1$\bar{1}$1] and Have a Line Direction of [1$\bar{1}$1] and Thus Are Pure Screw Dislocations.

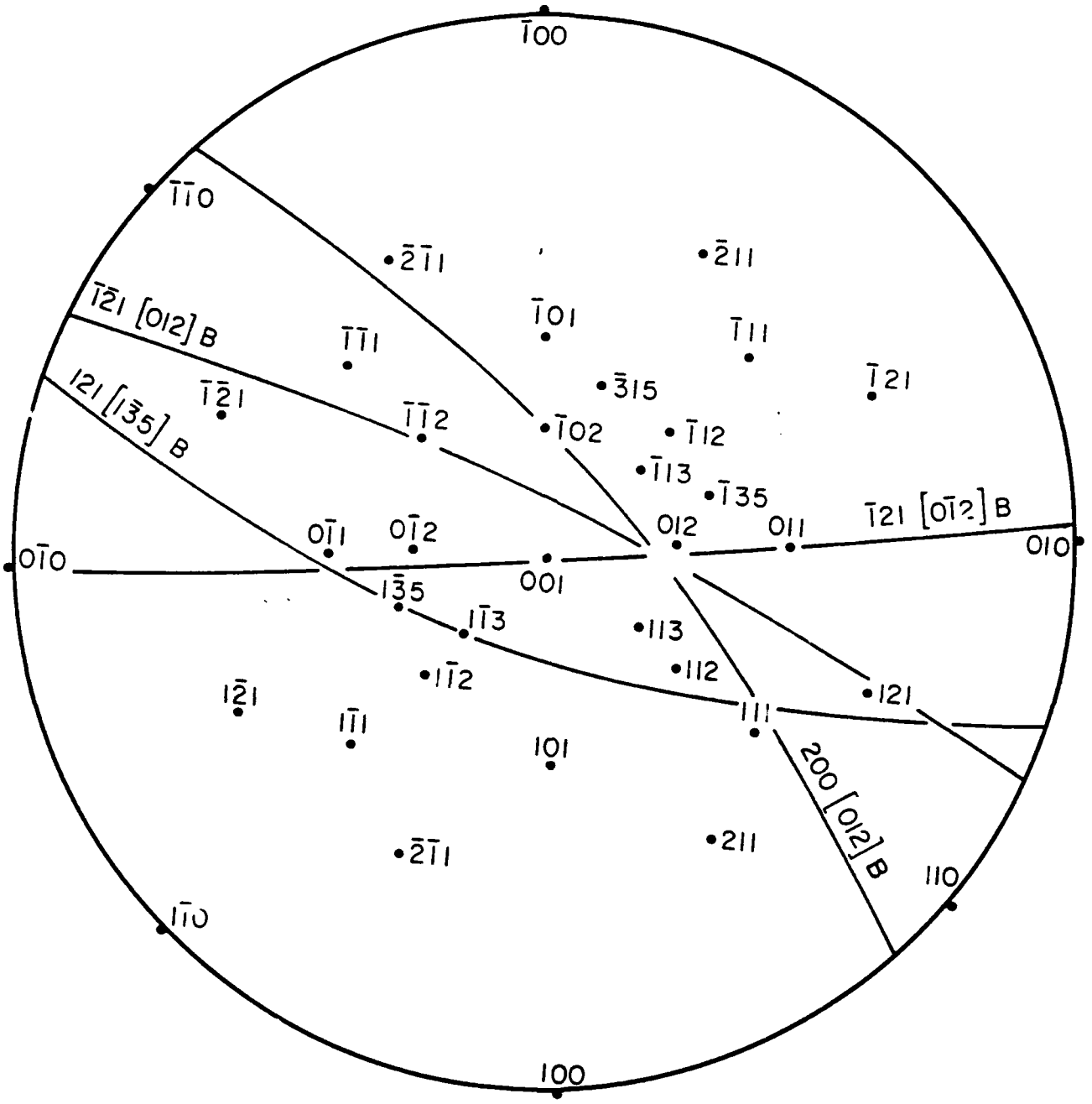

Figure 4b. Stereograms of the [100] Projection Showing the Intersection of Four Projected Planes Between the [012] and the [111] Zone Axis, Which Were Taken From the Projected Line Directions at Their Respective Beam Directions of the Dislocations Which Are Labelled B in Figure 3. These Dislocations Have a Burgers Vector of 1/2 [111] and Have a Line Direction Between [111] and [012] Which Makes Them Pure Screw Dislocations or They Have a Large Screw Component and Lie on the $(1\bar{2}1)$.

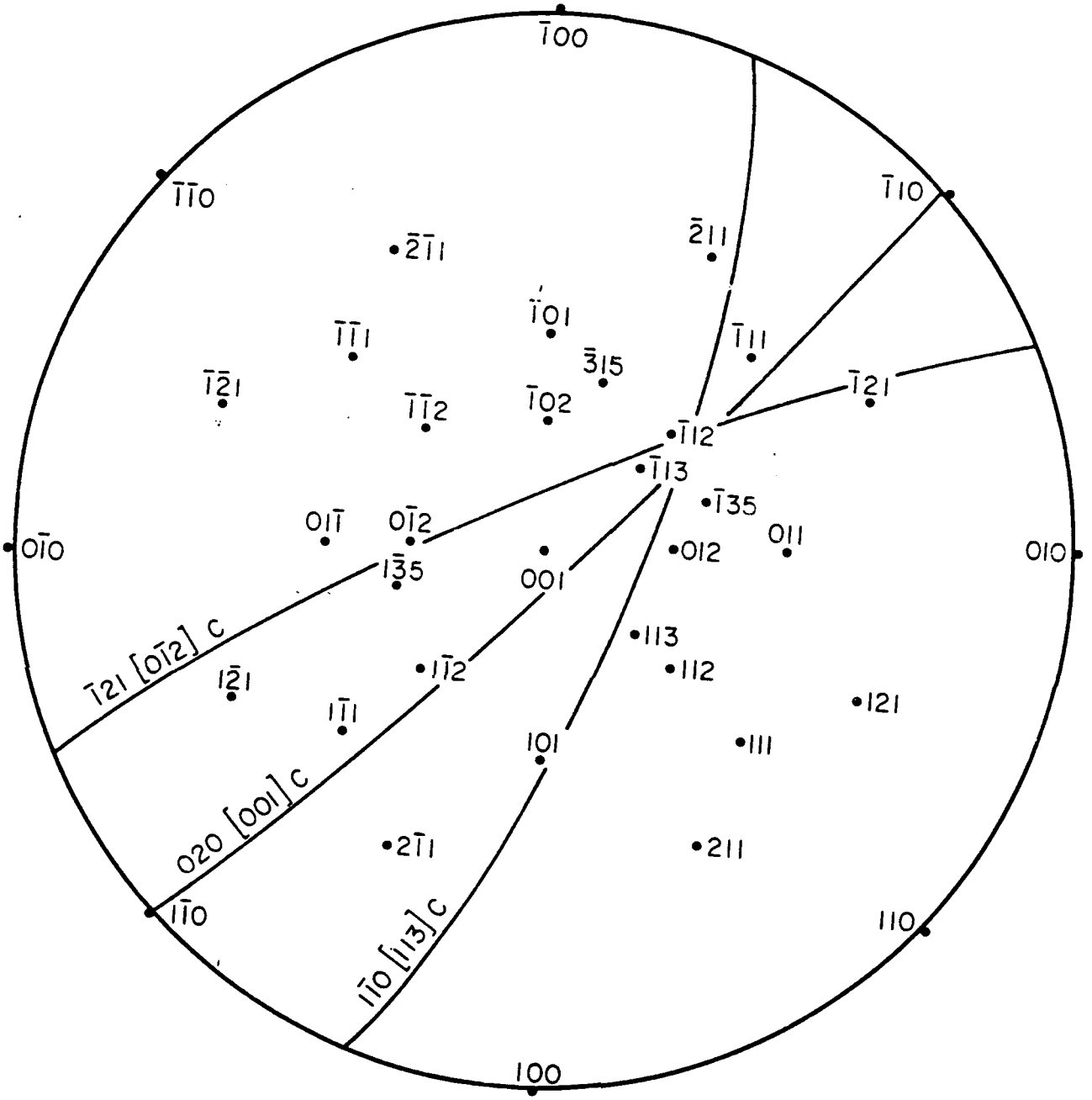

Figure 4c. Stereograms of the [100] Projection Showing the Intersection of Three Projected Planes Around the $[\bar{1}11]$ Zone Axis, Which Were Taken From the Projected Line Directions at Their Respective Beam Directions of the Dislocations Which Are Labelled C in Figure 3. These Dislocations Have a Burgers Vector of 1/2 $[\bar{1}11]$ and Have a Line Direction of $[\bar{1}12]$ and Thus Lie on the (110).

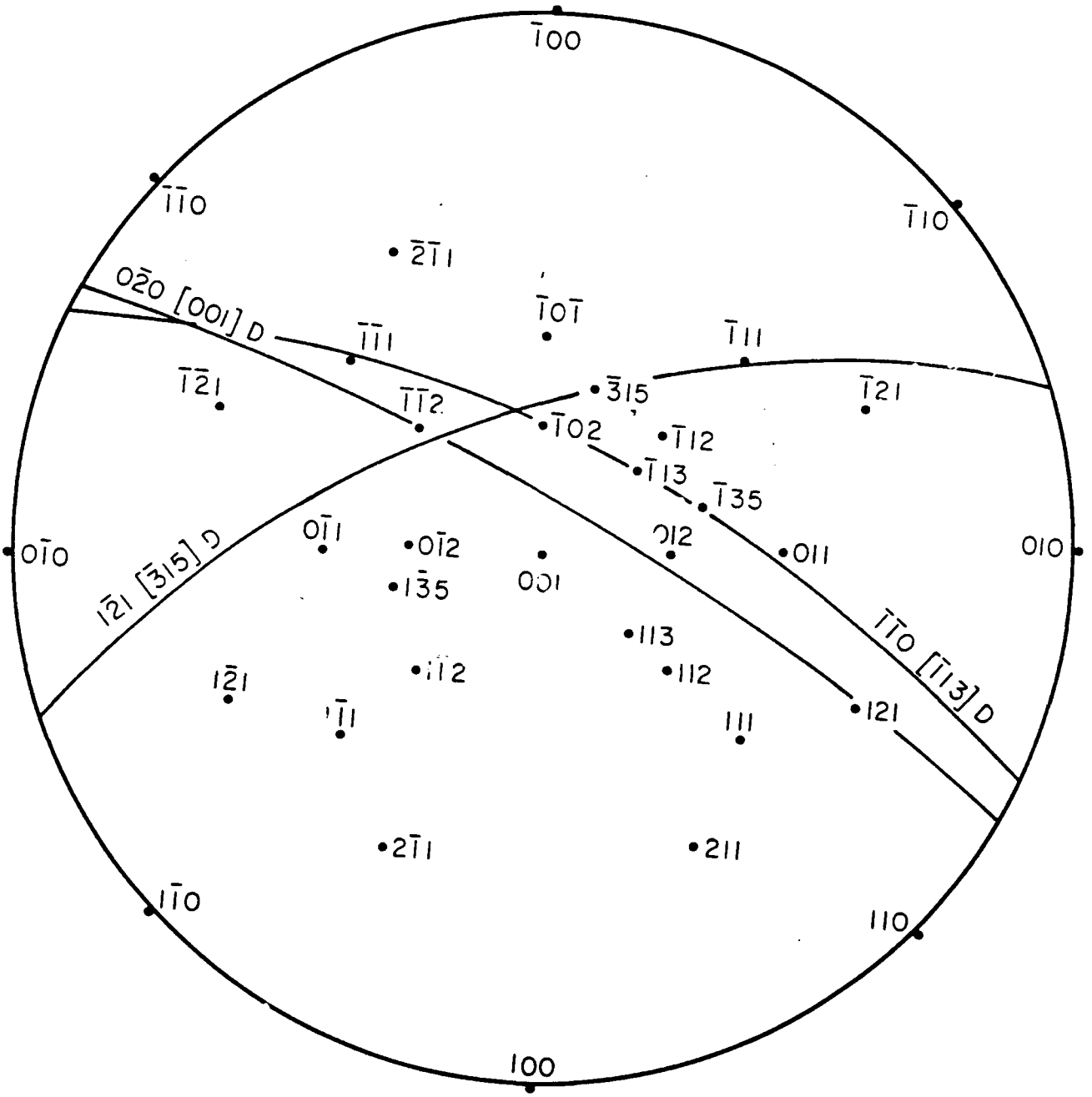

Figure 4d. Stereograms of the [100] Projection Showing the Intersection of Three Projected Planes Between the $[\bar{1}\bar{1}2]$, $[\bar{1}02]$, and the $[\bar{1}\bar{1}1]$ Zone Axis, Which Were Taken From the Projected Line Directions at Their Respective Beam Directions of the Dislocations Which Are Labelled D in Figure 3. These Dislocations Had a Burgers Vector of 1/2 $[\bar{1}\bar{1}1]$ and Thus Have a Large Screw Component.

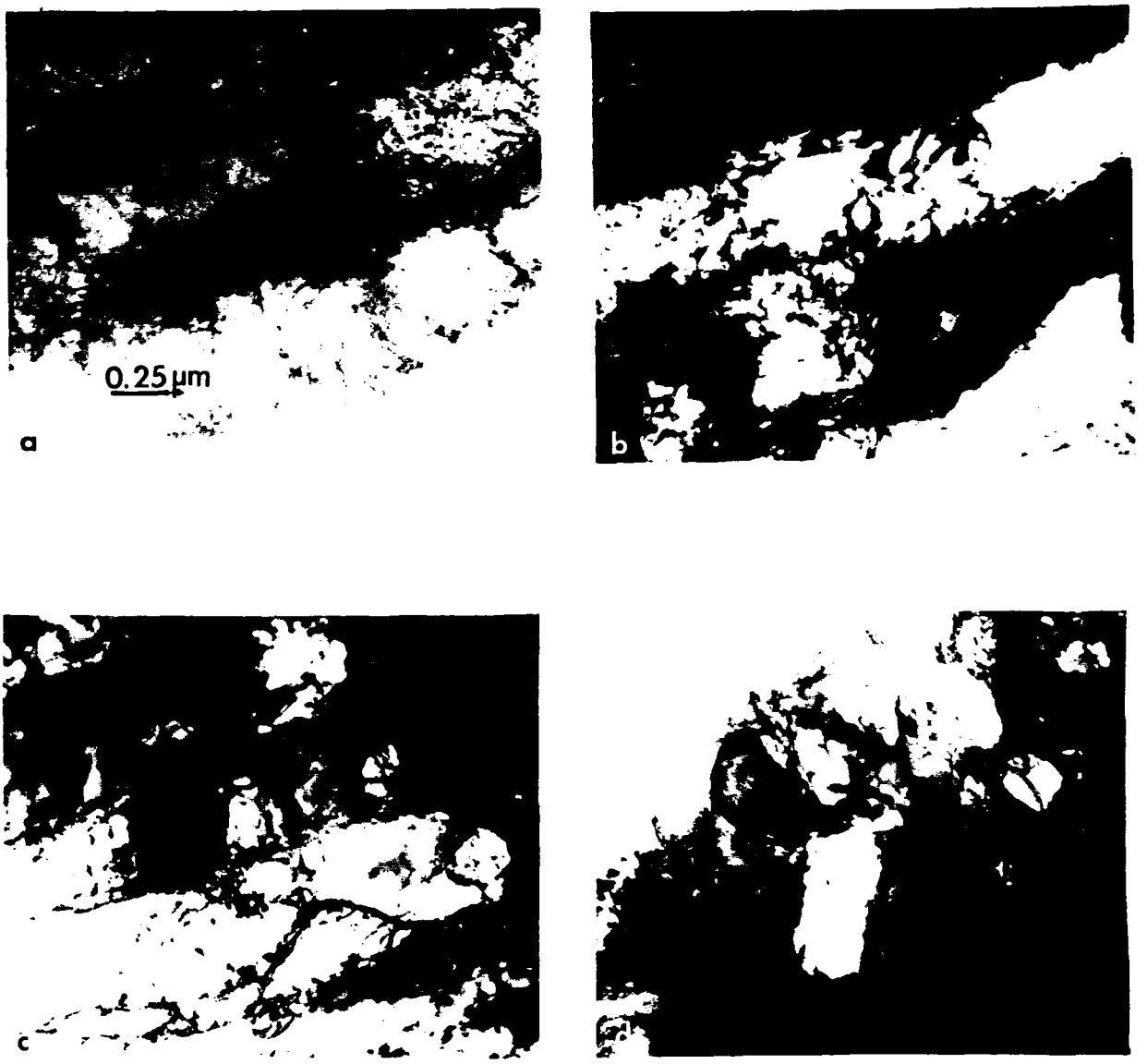

Figure 5. The General Microstructure of the Deformed [110] Penetrator Showing a) to c) Heavily Dislocated, Well-Defined, Elongated Grains and d) Some Recrystallization Which Has Produced Small Grains of Low Dislocation Density.

taken from a region close to those regions shown in Figure 5, is presented in Figures 6a–6j. Three similar types of dislocations, which have been labelled A, B, and C, dominate the microstructure. These dislocations are in and out of contrast for many diffraction vectors, and a summary is listed in Table 3. The dislocations which are labelled A are out of contrast for the diffraction vectors of $2\bar{1}1$ g [011], $\bar{1}10$ g [111], and $\bar{1}21$ g [101] and thus have b = 1/2 [$11\bar{1}$]. The dislocations which are labelled B are out of contrast for $21\bar{1}$ g [135], $10\bar{1}$ g [131], and $10\bar{1}$ g [101] and thus have b = 1/2 [$1\bar{1}1$]. The dislocations which are labelled C are out of contrast for $11\bar{2}$ g [021], $01\bar{1}$ g [011], $10\bar{1}$ g [131], $\bar{1}10$ g [111], and $10\bar{1}$ g [101] and thus have b = 1/2 [111]. The projected line directions of the dislocations labelled A and B, with respect to the diffraction vectors, are labelled in Table 4. The projected planes are plotted on the stereograms of Figures 7a–7b. It can be seen that the intersection of the projected planes produces u = [$11\bar{1}$] for the dislocations labelled A and u = [$1\bar{1}1$] for the dislocations labelled B. Thus these segments of dislocations A and B, which are very straight, are pure screw dislocations. However, these dislocations should be analyzed further. The $0\bar{1}1$ g [311] (i.e., Figure 6c) shows clearly that the dislocations labelled A and B have segments which are perpendicular to the dislocations overall length. The arrowed segments of the dislocations labelled A have u ~[131], which is also close to the [221]—see how they disappear for $\bar{1}01$ g [131], Figure 6i (i.e., they are in the [131] electron beam direction)—which makes them pure edge dislocations lying on the (211) or ($1\bar{1}0$) slip planes. The segments of the dislocations labelled B have u ~(311) (see how they disappear for $\bar{2}1\bar{1}$ g [011], Figure 6 g), which makes them pure edge dislocations lying on the ($21\bar{1}$), which is not far from the ($2\bar{1}1$) and ($1\bar{1}0$) slip planes of the dislocations labelled A. The habit planes for the dislocations labelled C were difficult to determine as their line directions were hard to follow.

3.3 [111]-Oriented Penetrator. General views of the deformation microstructure of a [111] penetrator (Figures 8a–8d) show subgrain boundaries with a high density, orderly array of dislocations. A complete analysis of a dislocation network, which was taken from a region close to that shown in Figure 8, is presented in Figures 9a–9f. Three types of dislocations which have been labelled A, B, and C dominate the microstructure. The dislocations labelled A are on both sides of the subgrain boundary. These dislocations are in and out of contrast for many diffraction vectors, and a summary is listed in Table 5. The dislocations which are labelled A, B, and C have a b = 1/2 [$11\bar{1}$], 1/2 [111], and 1/2 [$1\bar{1}1$], respectively. The projected line directions of the dislocations labelled A and B, with respect to the diffraction

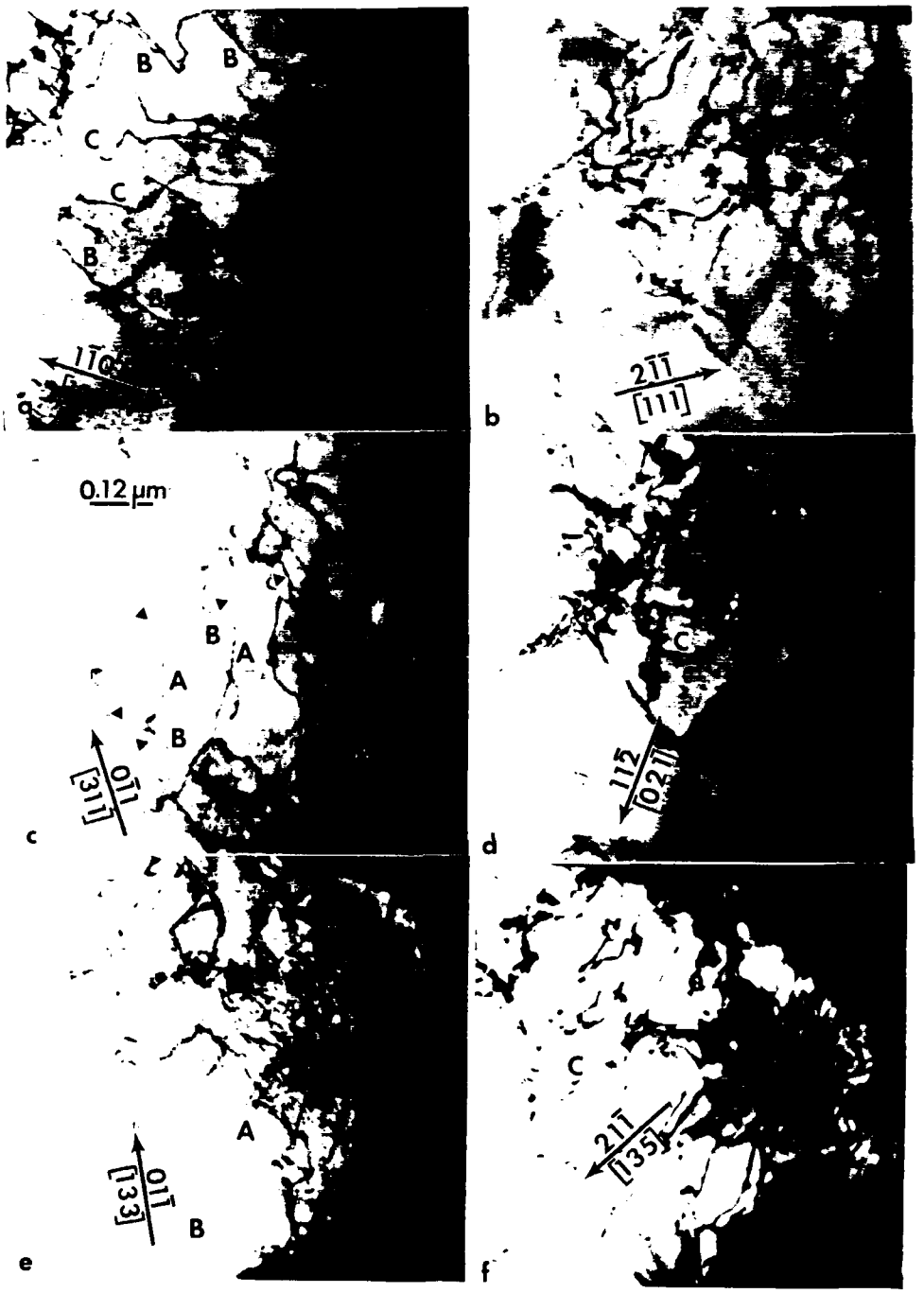

Figure 6. The Analysis of a Dislocation Network of a Region Close to Those Shown in Figure 5 From a [110] Penetrator Showing Many Two-Beam Electron Diffraction Conditions Which Put the Dislocations, Which Are Labelled A, B, and C, In or Out of Contrast. Note That c) Clearly Shows Segments of Dislocation Which Have Edge Character (Labelled by Arrows). Please See the Text and Table 3 and Table 4 for Further Information.

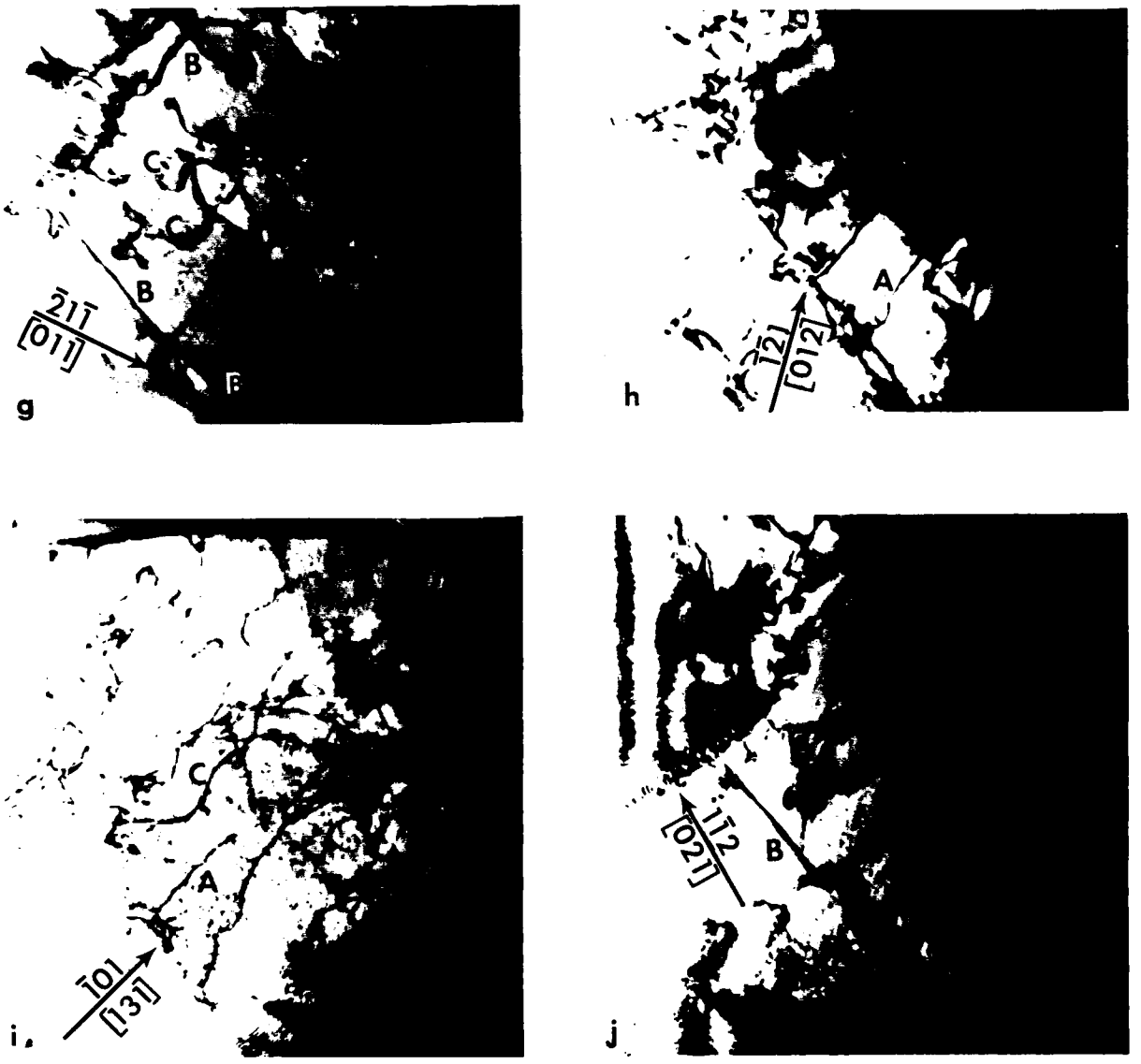

Figure 6. The Analysis of a Dislocation Network of a Region Close to Those Shown in Figure 5 From a [110] Penetrator Showing Many Two-Beam Electron Diffraction Conditions Which Put the Dislocations, Which Are Labelled A, B, and C, In or Out of Contrast. Note That c) Clearly Shows Segments of Dislocation Which Have Edge Character (Labelled by Arrows). Please See the Text and Table 3 and Table 4 for Further Information (Continued).

Table 3. Analysis of Dislocation Contrast for Various Diffraction Vectors
[110] Orientation, Specimen A1, Box 2, Film 1057–1102

±g, Diffraction Vector [Zone Axis]	Dislocation Segments + in contrast, - out of contrast ? unsure of contrast		
	A	B	C
$1\bar{1}2$ [021]	+	+	-
$1\bar{1}2$ [021]	+	+	+
$2\bar{1}1$ [011]	-	+	+
$01\bar{1}$ [011]	+	+	-
$21\bar{1}$ [135]	+	-	+
$12\bar{1}$ [012]	+	+	?
$10\bar{1}$ [131]	+	-	-
$\bar{1}10$ [111]	-	+	-
$\bar{2}11$ [111]	+	+	+
$0\bar{1}1$ [311]	+	+	-
$\bar{1}12$ [311]	?	?	+
$10\bar{1}$ [101]	+	-	-
$\bar{1}21$ [101]	-	+	+
2x<u>B</u>	<$11\bar{1}$>	<$1\bar{1}1$>	<111>

Table 4. Projected Line Direction for Various Dislocations With Respect to Diffraction Vectors
[110] Orientation, Specimen A1, Box 2, Film 1057–1102

±g, Diffraction Vector [Zone Axis]	Dislocation Segments Angle of Rotation (°) cw clockwise ccw conterclockwise	
	A	B
$1\bar{1}2$ [021]	20 cw	63 ccw
$1\bar{1}2$ [021]	72 cw	12 ccw
$2\bar{1}1$ [011]	–	24 cw
$01\bar{1}$ [011]	48 cw	31 ccw
$21\bar{1}$ [135]	11 ccw	–
$12\bar{1}$ [012]	–	–
$10\bar{1}$ [131]	0	–
$\bar{1}10$ [111]	–	29 cw
$\bar{2}11$ [111]	52 ccw	58 cw
$0\bar{1}1$ [311]	36 cw	20 ccw
$\bar{1}12$ [311]	41 ccw	–
$10\bar{1}$ [101]	15 ccw	–
$\bar{1}21$ [101]	–	–

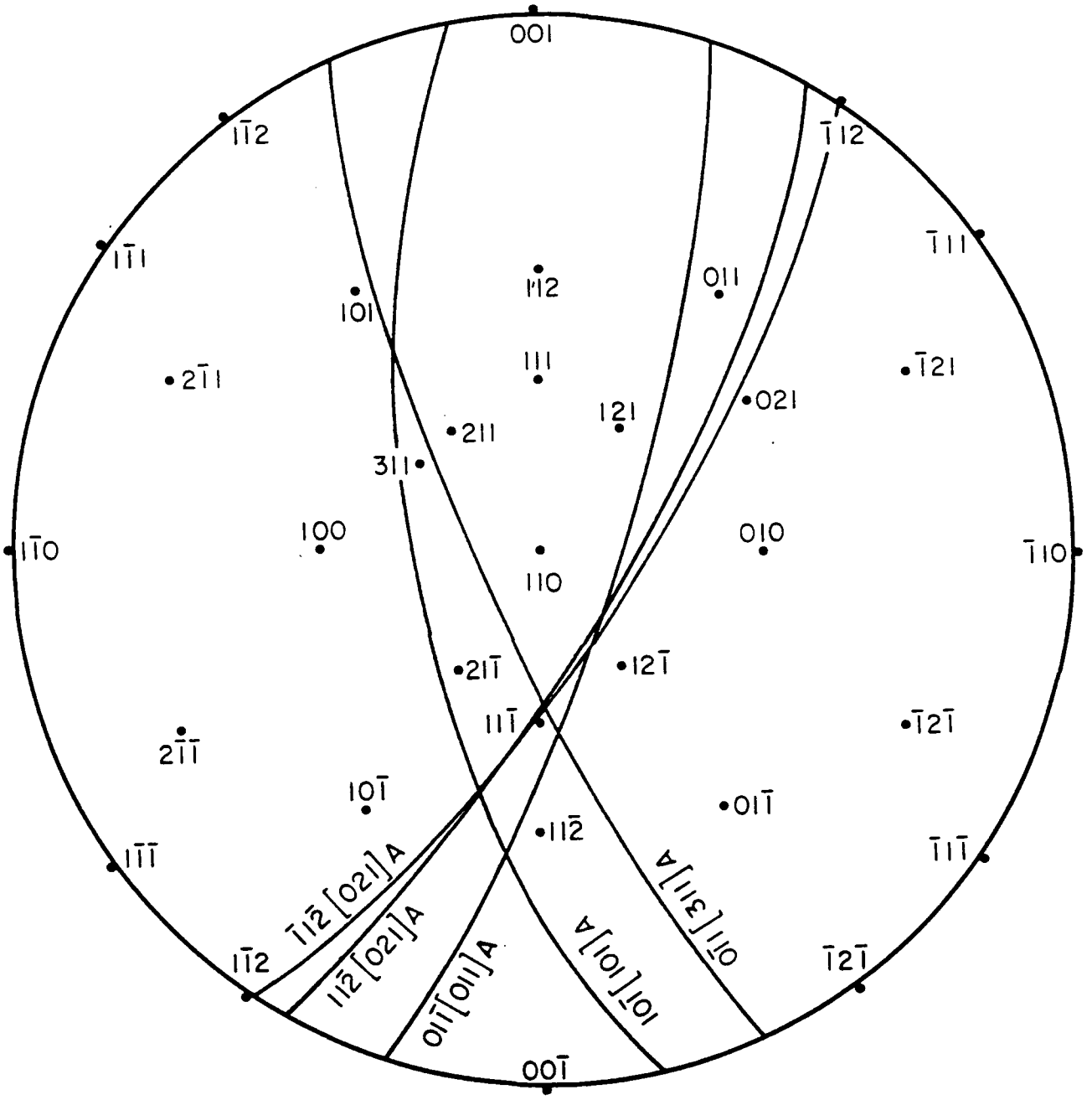

Figure 7a. Stereograms of the [110] Projection Showing the Intersection of Five Projected Planes Close to the [11$\bar{1}$] Zone Axis, Which Were Taken From the Projected Line Direction at Their Respective Beam Directions of the Dislocations Which Are Labelled A in Figure 6. These Dislocations Had a Burgers Vector of 1/2 [11$\bar{1}$] and Thus Have a Large Screw Component.

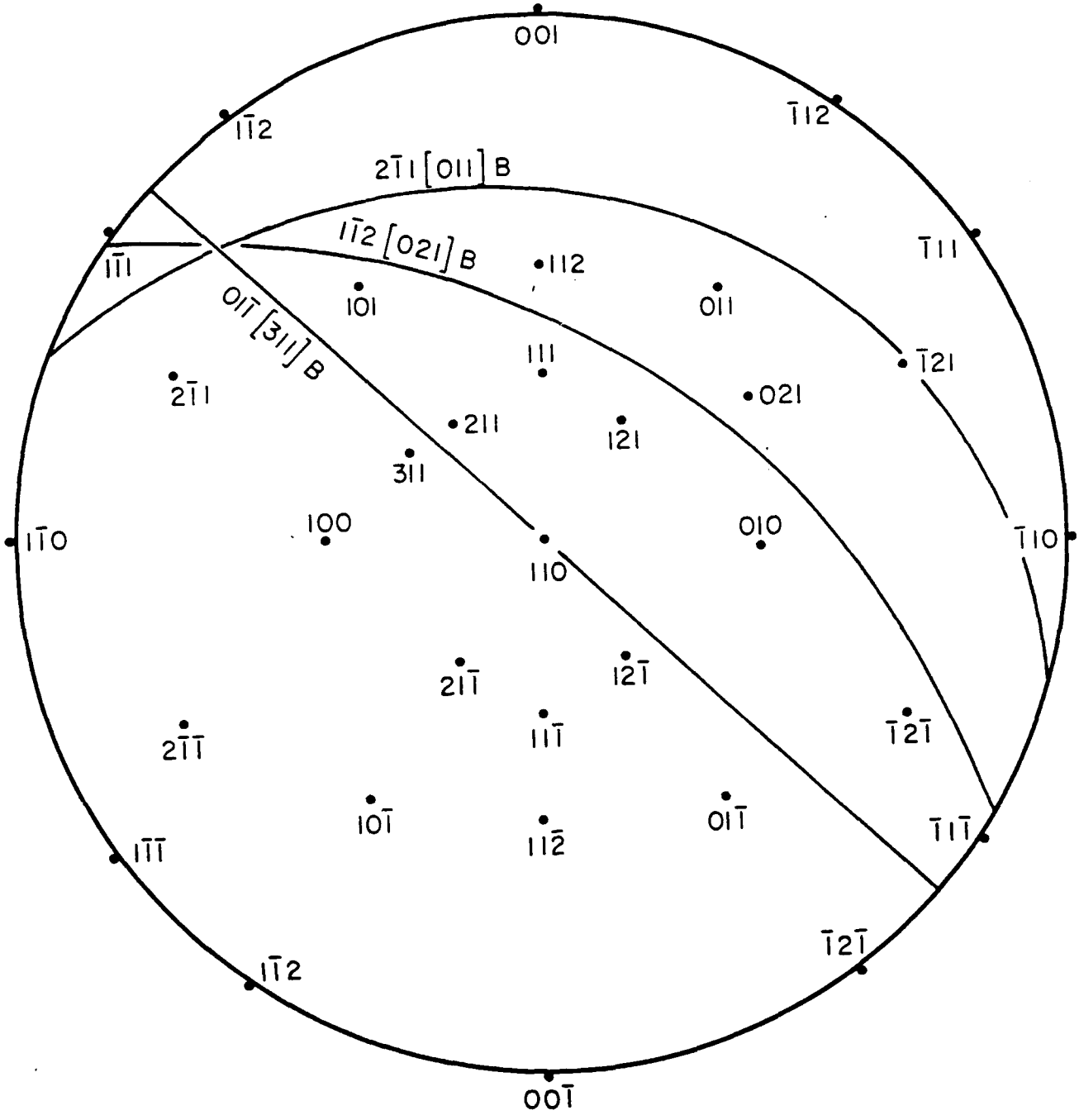

Figure 7b. Stereograms of the [110] Projection Showing the Intersection of Three Projected Planes Close to the $[1\bar{1}1]$ Zone Axis, Which Were Taken From the Projected Line Directions at Their Respective Beam Directions of the Dislocations Which Are Labelled A in Figure 6. These Dislocations Had a Burgers Vector of 1/2 $[1\bar{1}1]$ and Thus Have a Large Screw Component.

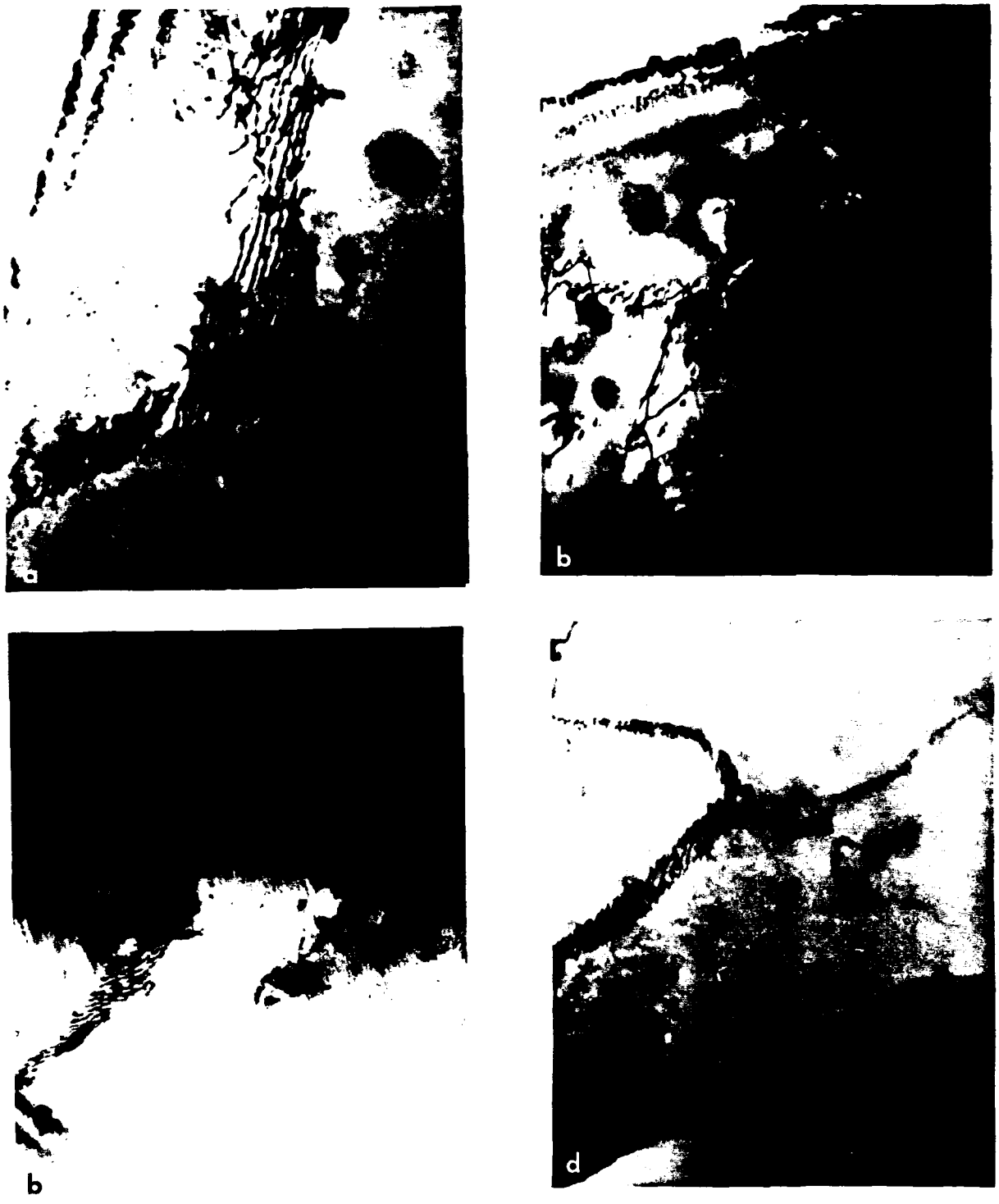

Figure 8. The General Microstructure of the Deformed [111] Penetrator Showing an Orderly Arrangement of Dislocations Which Have Formed a High Density of Dislocations at the Subgrain Boundaries.

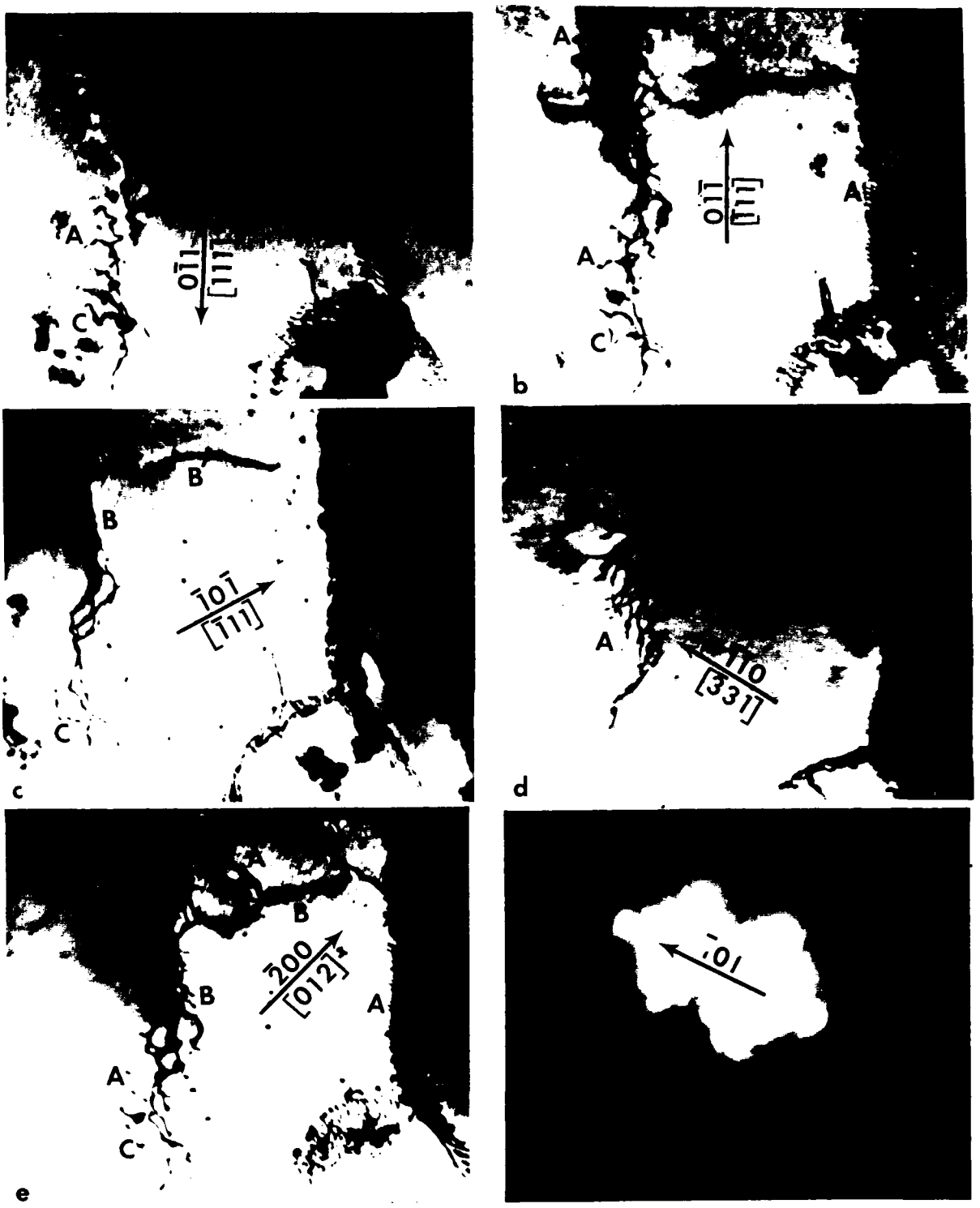

Figure 9. The Analysis of a Dislocation Network From a [111] Penetrator Showing Many Two-Beam Electron Diffraction Conditions Which Put the Dislocations, Which Are Labelled A, B, and C, In or Out of Contrast. A Two-Beam Electron Diffraction Pattern Is Shown in f). Please See the Text and Table 5 and Table 6 for Further Information.

Table 5. Analysis of Dislocation Contrast for Various Diffraction Vectors
[111] Orientation, Specimen K1, Box 1, Film 452–463

±g, Diffraction Vector [Zone Axis]	Dislocation Segments + in contrast, - out of contrast ? unsure of contrast		
	A	B	C
101 [$\bar{1}$11]	-	+	+
0$\bar{1}$1 [$\bar{1}$11]	+	-	+
200 [012]	+	+	+
110 [$\bar{3}$31]	+	+	-
2x<u>B</u>	<11$\bar{1}$>	<111>	<1$\bar{1}$1>

vectors, are listed in Table 6. The projected planes are plotted on the stereograms of Figures 10a–10b. The intersection of the projected planes can be seen to be very close to the direction of b. Thus, the dislocations labelled A and B are either pure screw dislocations or mixed dislocations with a large screw component.

Table 6. Projected Line Direction for Various Dislocations With Respect to Diffraction Vectors
[111] Orientation, Specimen K1, Box 1, Film 452–463

±g, Diffraction Vector [Zone Axis]	Dislocation Segments Angle of Rotation (°) cw clockwise ccw conterclockwise	
	A	B
101 [$\bar{1}$11]	–	53 ccw
0$\bar{1}$1 [$\bar{1}$11]	63 ccw	–
200 [012]	90 cw	65 cw
110 [$\bar{3}$31]	60 ccw	50 cw

4. DISCUSSION

A significant amount of research has been performed on the deformation behavior of V single crystals. Rose, Ferriss, and Wulff (1962) looked at the effect of orientation on the stresses for yielding and plastic flow and showed that the [100] and [111] orientations work

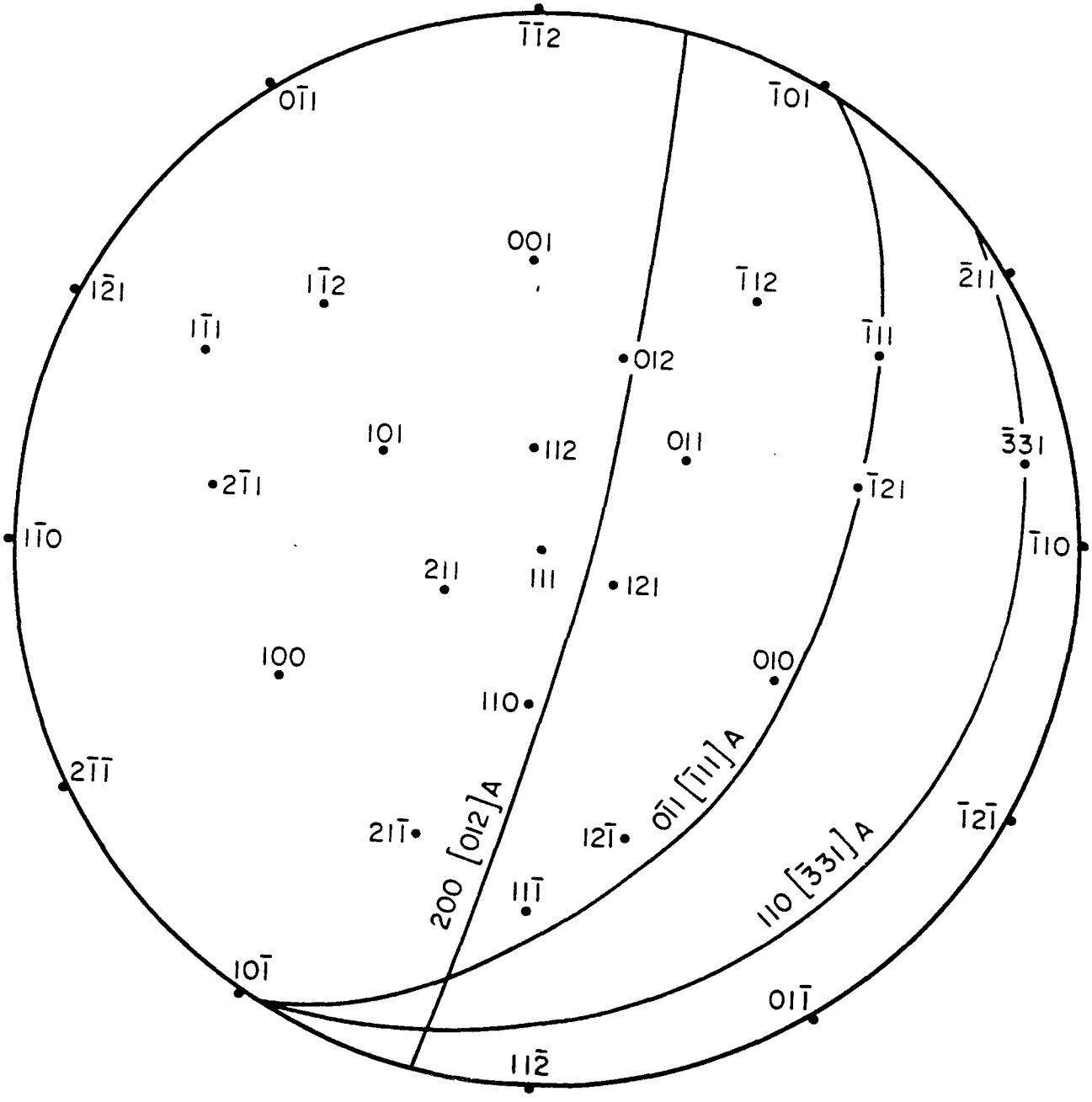

Figure 10a. Stereograms of the [111] Projection Showing the Intersection of Three Projected Planes Close to the [111] Zone Axis, Which Were Taken From the Projected Line Directions at Their Respective Beam Directions of the Dislocations Which Are Labelled A in Figure 9. These Dislocations Had a Burgers Vector of 1/2 [111] and Thus Have a Large Screw Component.

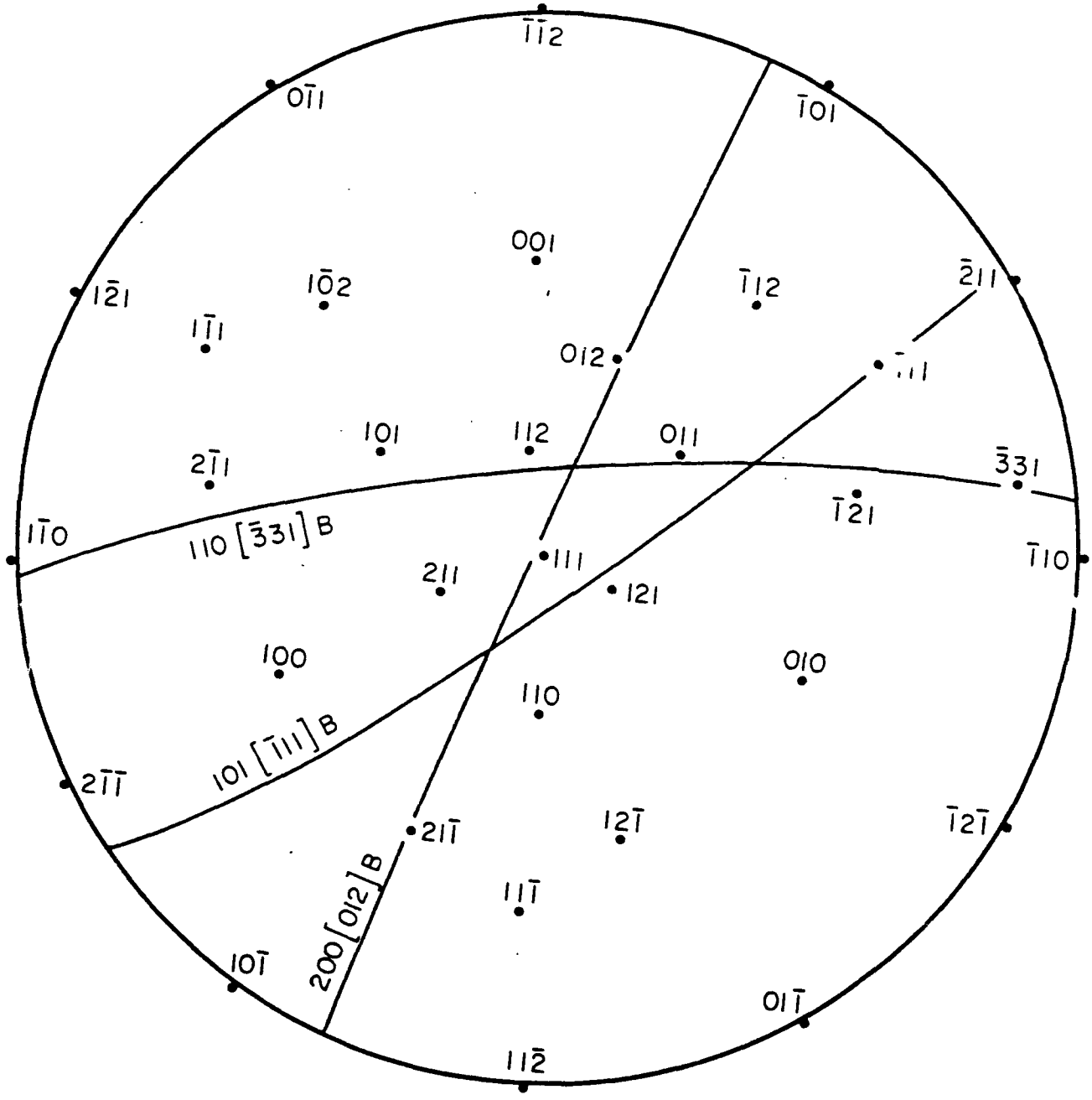

Figure 10b. Stereograms of the [111] Projection Showing the Intersection of Three Projected Planes Close to the $[11\bar{1}]$ Zone Axis, Which Were Taken From the Projected Line Directions at Their Respective Beam Directions of the Dislocations Which Are Labelled B in Figure 9. These Dislocations Had a Burgers Vector of 1/2 $[11\bar{1}]$ and Thus Have a Large Screw Component.

hardened whereas the [110] orientation did not. They also gave plausible interpretations as to the differences in yielding behavior. Taylor (1965) looked at the slip systems operable as a function of temperature and, not surprisingly, found that all expected slip systems were operable at temperatures >1,370° C with slip in the <111> directions being dominant (i.e., screw dislocations) at high deformations (>38%).

4.1 Analysis of Dislocations at Subgrain Boundaries. A significant difference between the three types of penetrators (i.e., the single crystals of [100], [110], and [111]) was the morphology of the dislocation networks which formed the subgrain boundaries. The [100]-oriented penetrator had a disorderly, tangled array of dislocations. The [111]-oriented penetrator had an orderly array of dislocations, and the [110]-oriented penetrator was in between the two extremes. The dislocation networks at the subgrain boundaries are indicative of their different dislocation generation mechanisms (and thus deformation mechanism). Even though most of the dislocations identified had large screw components and Burgers vectors of 1/2 <111>, their general morphology (i.e., their straight, curved, or wavey appearance) indicates how they were formed. For example, in the [110] penetrator, straight screw dislocations were identified as having pure edge dislocations at their ends. An edge dislocation, when passing through a crystal, will leave behind a straight, screw dislocation. When screw dislocations or mixed dislocations with a large screw component pass through a crystal, they tend to produce bowed or wavey fronts which were seen with the [100] and [111] penetrators.

4.2 General Microscopic Deformation. When considering deformation by slip on specific planes the critical resolved shear stress (CRSS) must be considered. Table 7 shows the CRSS for slip of dislocations having b = 1/2 <111> on {110} and {112} slip planes at the penetrator orientations of [100], [110], and [111]. It can be seen that the [100] orientation has four symmetrical slip directions, 45° apart (also see the [100] stereographic projection, Figure 4a), operative with four {110} and two {112} slip planes which have a reasonably large CRSS of 0.41 to 0.47, respectively. The dislocations on these planes have a large screw component. The stress on a pure screw dislocation at the [100] orientation would be cos 54.7° = 0.58. Thus, the [100] orientation has many dislocation systems which are favorable for deformation and which all have a large screw component. They would produce a dense, tangled array of wavey dislocations which is consistent with the results.

Table 7. Critical Resolved Shear Stress Factors on Slip Planes for Various Orientation Penetrators

Orientation	No. of Slip Directions	[111] Slip Angle, 0	No. of (110) Slip Planes[a]	(110) Angle, Y	No. of (112) Slip Planes[a]	(112) Angle, Y	CRSS
[100]	4	54.7	4	45	—	—	0.41
		54.7	2	90	—	—	0.00
		54.7	—	—	2	35.3	0.47
		54.7	—	—	4	65.9	0.24
[111]	3	70.5	4	35.3	—	—	0.27
		70.5	2	90	—	—	0.00
		70.5	—	—	1	19.5	0.31
		70.5	—	—	2	61.9	0.16
	1	0.00	6	90	—	—	0.00
		0.00	—	—	6	90	0.00
[110]	2	35.3	4	60	—	—	0.41
		35.3	2	90	—	—	0.00
		35.3	—	—	2	54.7	0.47
		35.3	—	—	4	73.2	0.24
	2	90.0	6	0, 60	—	—	0.00
		90.0	—	—	6	30, 90	0.00

[a] for each slip direction.

In Table 7, it can be seen that the [111] orientation has three symmetrical slip directions, 60° apart (also see Figure 10a), operative with four {110} and two {112} slip planes which do not have very large CRSS values of 0.27 and 0.3, respectively. The stress on the pure screw dislocations at these [111] orientations would not be much larger than these CRSS values (i.e., cos 70.5° = 0.33). However, the stress component for the screw dislocation which is normal to the penetrator orientation is cos 0° = 1. Thus, the [111] orientation does not have any favorable slip system for deformation but does have a highly favorable orientation for the formation of one type of screw dislocation. Deformation by only one screw dislocation system is unlikely since the resultant rotation of the crystal is perpendicular to the line direction, u, which produces a nonconservative motion of the crystal (i.e., the crystal would have to form a free surface or crack in order to rotate). The stress induced by this nonconservative motion invokes one or more screw dislocations which are at or nearly perpendicular to this screw dislocation system. This is illustrated in Figure 11. This mechanism of deformation has evidently occurred in the [111]-oriented penetrator and is entirely consistent with the results.

In Table 7 it can be seen that the [110] orientation has only two slip directions (also see Figure 7a), operative with four {110} and two {112} slip planes which have fairly large CRSS values of 0.41 and 0.47, respectively. The stress on the pure screw dislocations at these [111] orientations would be much larger (i.e., cos 35.3° = 0.82). However, screw dislocations may not dominate the deformation of the [110] penetrator like the [111]-oriented crystal for two reasons—namely, the stress components in the [111] directions are less, 0.82 < 1, and the stress which is necessary for dislocation motion (i.e., the peierls stress) is less for slip than for motion of screw dislocations in b.c.c. materials (Cottrel 1953). It is apparent from the analysis of the [110]-oriented penetrator that slip by pure edge dislocations is operative. As well, it is apparent from viewing the [110]-oriented penetrator (Figure 12b) that the penetrator has reoriented, and active slip on the $[1\bar{1}0]$ plane has occurred. The reorientation has occurred because of the imbalance in stress relief caused by two slip directions being inoperative and probably due to the high stresses and temperatures invoked during penetration. Slip on the $[1\bar{1}0]$ by either [111] or $[11\bar{1}]$ slip direction produces pure edge dislocations. This analysis is entirely consistent with the results of the [110] penetrator. However, the [110] penetrator also appears (Figure 12b) to have [111]-type deformation where it has skewed ~35° from the [110] axis (i.e., deformation by screw dislocations dominate). This type of deformation was not seen by TEM and should be investigated.

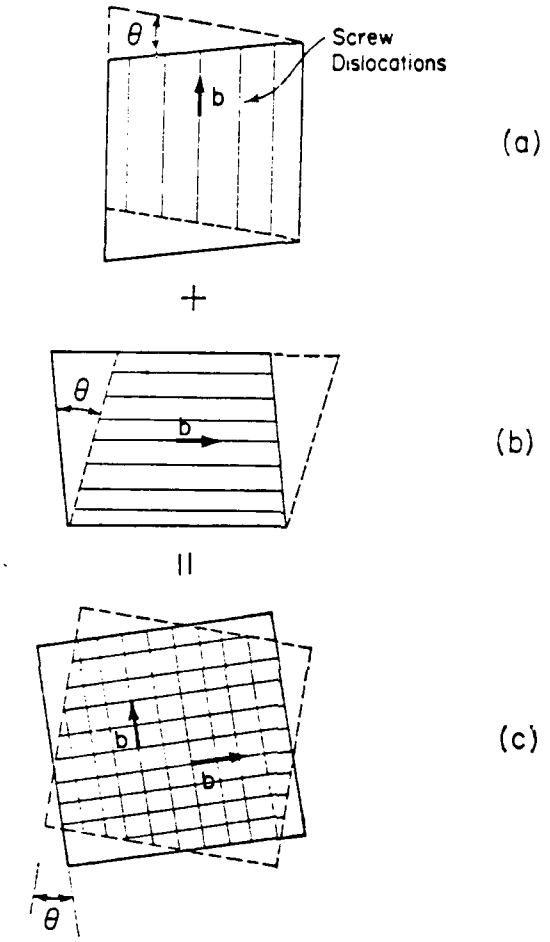

Figure 11. A Square Crystal Deformed by (a) a Vertical Set of Screw Dislocations; (b) a Horizontal Set of Screw Dislocations; and (c) Both Sets of Screw Dislocations. (Weertman and Weertman 1965).

In the three types of penetrators (i.e., the single crystals of [100], [110], and [111]), dislocations were found with Burgers vectors of 1/2 <111>. No other type of defect such as dislocations having b = [100] or b = [220], twins, or stacking faults which could produce deformation was found. Even though these defects were not found, deformation by crack nucleation and growth is expected to occur by the reaction,

$$a/2\,[111] + a/2\,[1\bar{1}\bar{1}] \rightarrow a\,[100], \qquad (1)$$

since cracks on the {100} are clearly evident in the residual penetrator material as shown in Figures 12a–12c. The [100]- and [111]-oriented penetrators are capable of forming these dislocations with Burgers vectors perpendicular to the tensile axis and thus forming cracks via Cottrell's mechanism (Figure 13). However, the [110]-oriented penetrator does not have a perpendicular set of {100}; although these dislocations could form, they may nucleate fracture by forcing <111>, <100>, or <220> dislocations of like sign together to nucleate a crack (Figure 14).

4.3 Recrystallization. Recrystallization of the grains removed the dense dislocation networks and was seen in material which was on the order of hundreds of micrometers from regions which appeared to have freshly deformed. The regions which are deforming at or near the penetrator/RHA interface are at a relatively high temperature (initial results show melted Fe in the cracks of the penetrator), and there is sufficient energy to undergo recrystallization. It is likely that recrystallization of a given piece of deforming material occurs several times during its course of flow from the head of the penetrator to the side wall of the cavity. The crystallographic relationship between the penetrator axis and material which has flowed to the cavity walls should be significantly destroyed by recrystallization.

4.4 Macrodeformation of Penetrators and Mass Flow. The dependence of the penetrators' deformation on crystallographic orientation is clearly shown in Figures 12a–12c. The [100]-oriented penetrator deforms symmetrically on many different <111>{110} and <111>[112] systems, and many cracks on the {100} planes which are perpendicular to the penetrators' axis are visible. Once the [100] penetrator material flows around the penetrators' head to an angle of ~55°, deformation by <111> screw dislocations (which is the same deformation mechanism as the [111] penetrator) begins to occur, and these flow lines are

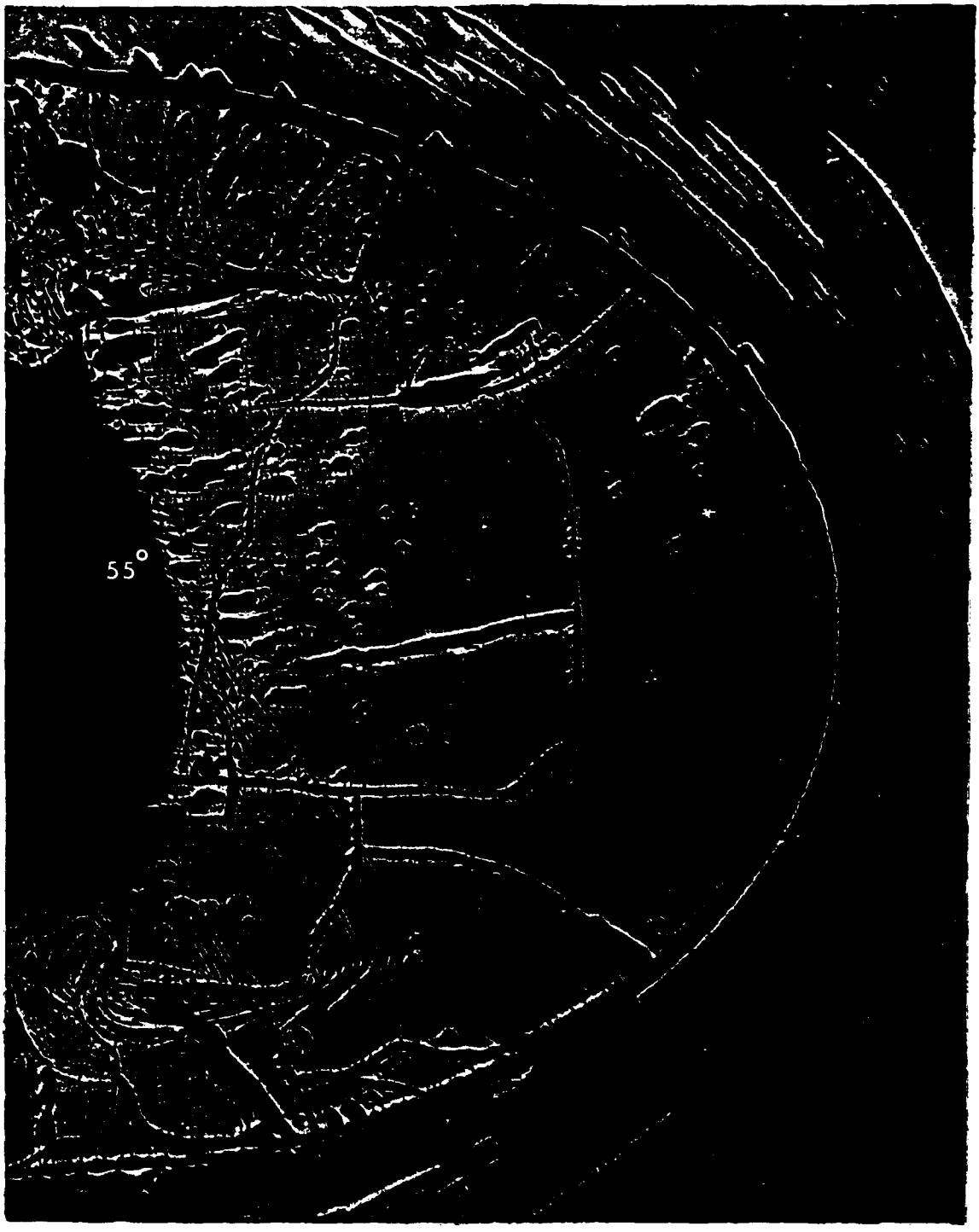

Figure 12a. Residual Material From a [100]-Oriented Penetrator Fired Into RHA. Note the Formation of Slip Lines Which Are Similar to Those Seen in the [111] Penetrator (Figure 12c) at Around 55° to the Penetration Axis. See Text.

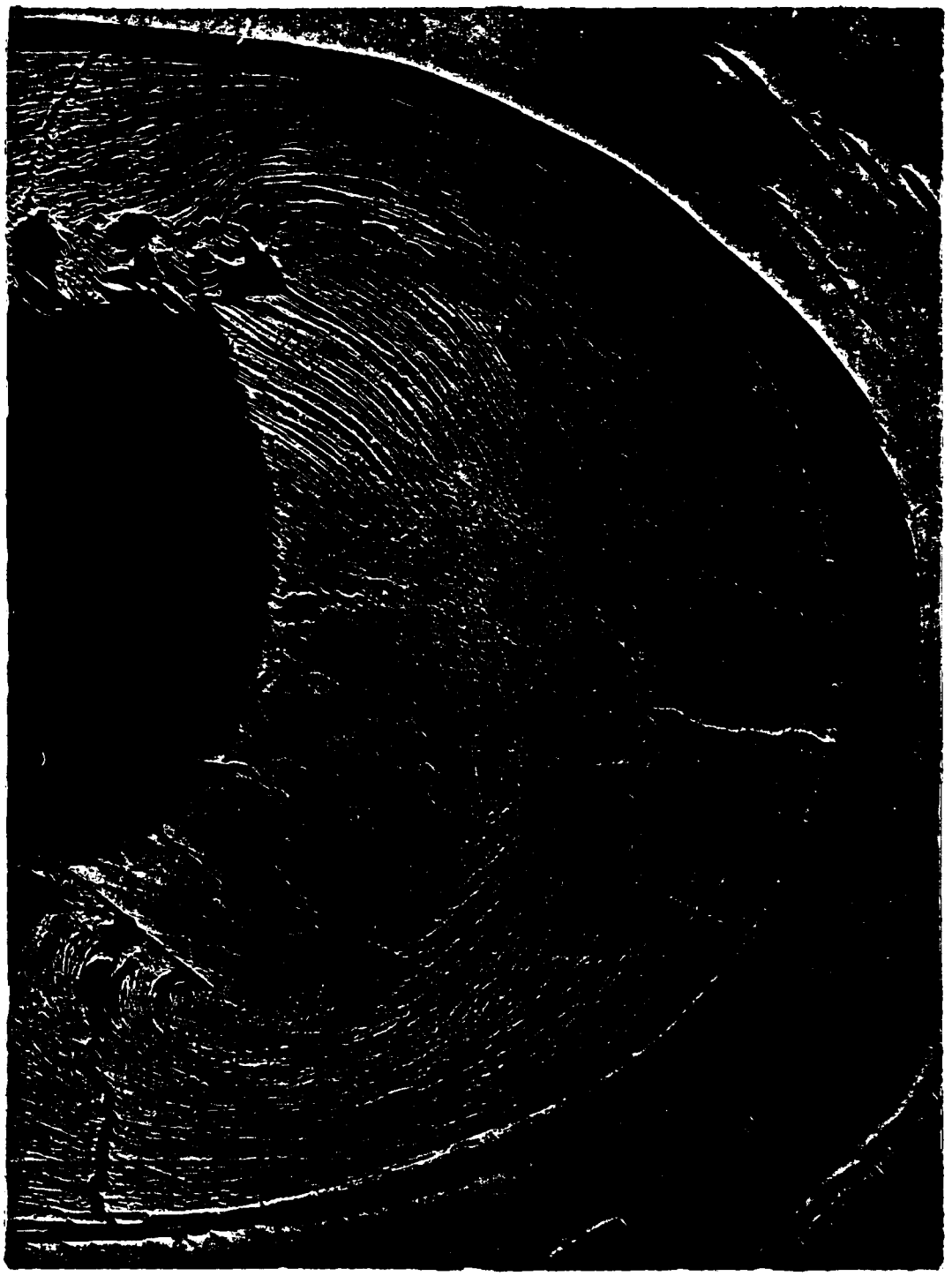

Figure 12b. Residual Material From a [110]-Oriented Penetrator Fired Into RHA. Note Reorientation of Residual Penetrator so That the [1$\bar{1}$0] Is Parallel to the Penetration Axis. See Text.

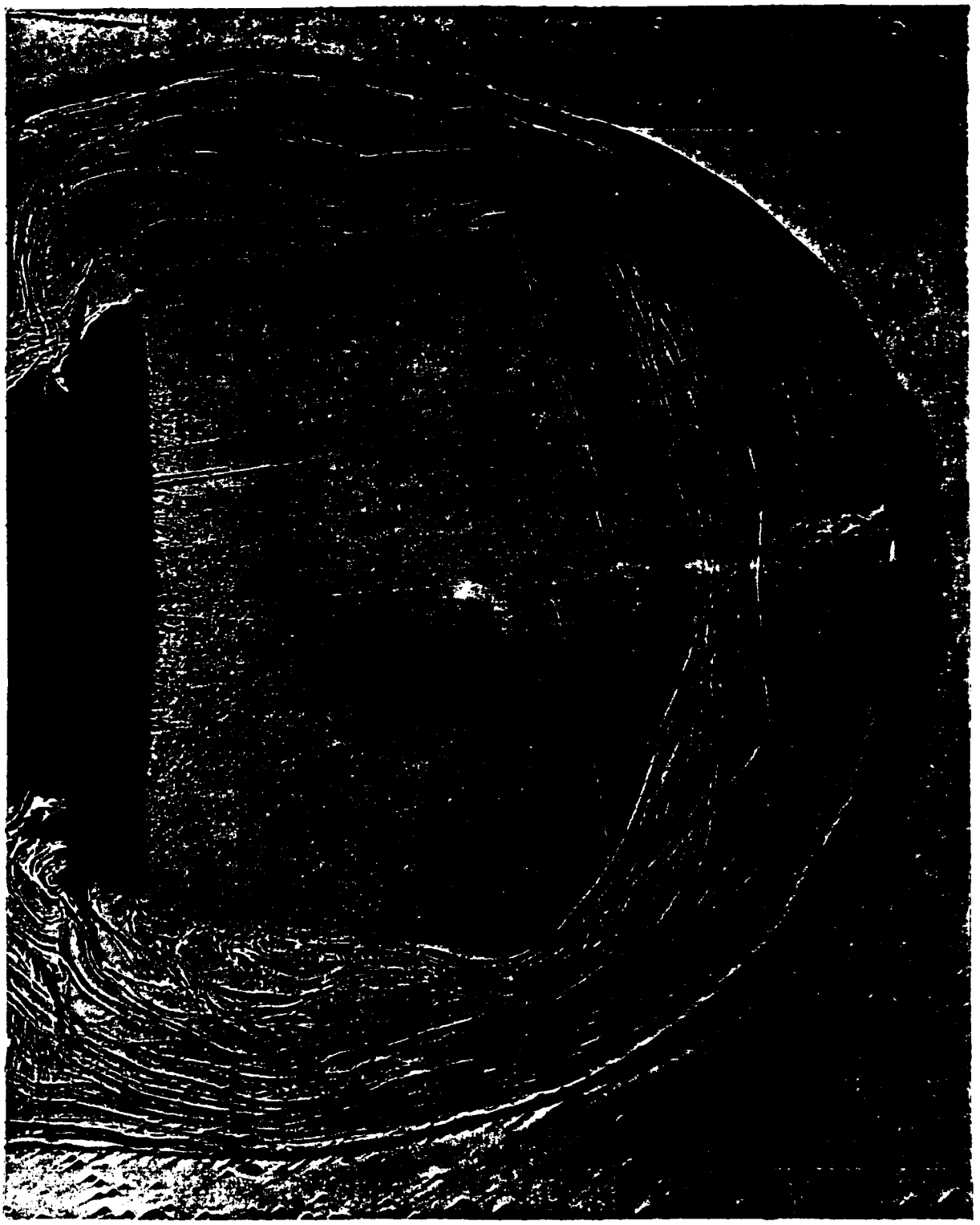

Figure 12c. Residual Material From [111]-Oriented Penetrator Fired Into RHA. Note Slip Lines of Differently Oriented Layers of Material.

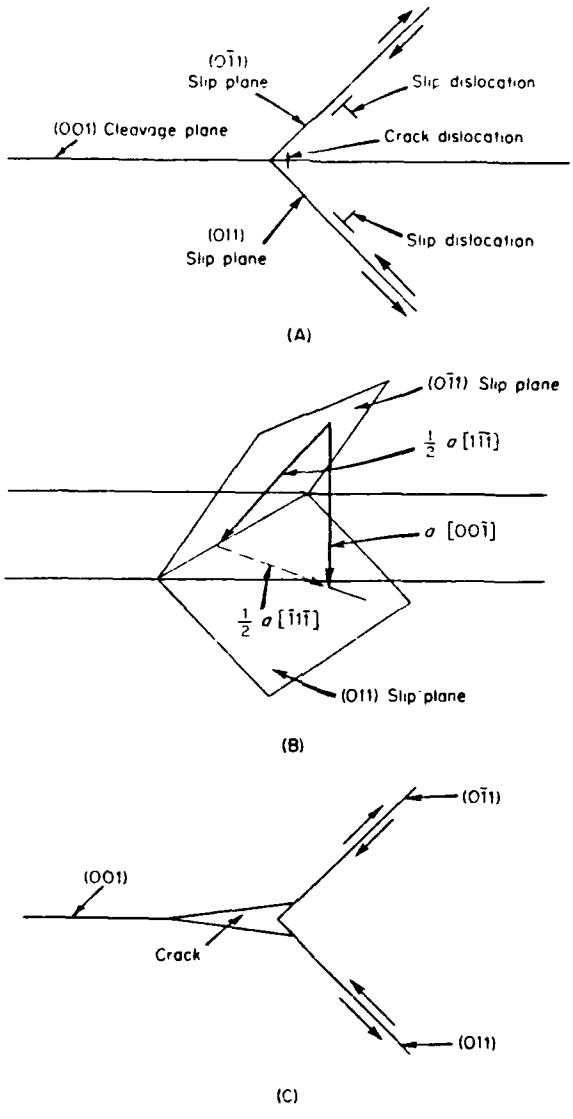

Figure 13. Cottrell's Dislocation Intersection Mechanism to Explain {100} Crack Nuclei in b.c.c. Crystals Where a) Shows Two Dislocations Combining to Form a Crack Dislocation, b) the Additions of the Burgers Vectors, and c) the Orientation of the Crack.

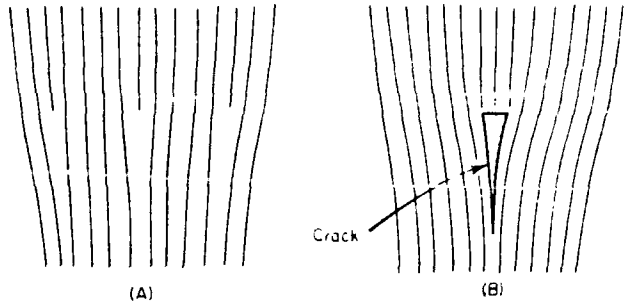

Figure 14. The Forcing Together of Edge-Type Dislocations of the Same Sign to Produce a Crack Nuclei.

clearly present in Figure 12a. The [110]-oriented penetrator which does not have symmetrical deformation in all directions, skews to one side where slip on the $(1\bar{1}0)$, which is parallel to the [110], can be clearly seen to occur (Figure 12b). Cracks in the [110] penetrator are not on any clearly defined {100} plane. The [111] penetrator, which has symmetrical deformation, clearly shows flow of material to the sides of the penetrator head. Flow lines closer to the tip of the penetrator/RHA interface would be at a high temperature and would be expected to be deformed (reoriented) greater than that material below it (i.e., the material closer to the residual penetrator). This deformation difference results in the formation of flow lines during etching. The flow of material at the top of the penetrator is away from the penetrators' axis, which is consistent with the formation of screw dislocations having b in the axis of the penetrator and one or more screw dislocations with b perpendicular to the penetrators' axis. The formation of cracks appears to be on the {100} planes located ~55° to the axis of the penetrator.

The general deformation mechanism and, thus, mass transfer from the penetrator to the walls of the cavity are given by the following description. The dislocations polyganized the single-crystal penetrators by forming grain boundaries. The dislocations thread their way through the crystal and formed dense arrays or subgrain boundaries, and, eventually, they formed elongated grains with a high density of dislocations within the grains. The flow of

dislocations along these subgrain and grain boundaries produce a mass transfer in a direction within the plane of the boundary. The mass transfer along the subgrain boundaries reorients the grains to form well-defined grains and boundaries. Further mass transfer along the grain boundaries results in the grains becoming elongated in the direction of mass flow, similar to that of rolled or forged material.

4.5 Ability of Penetrator to Penetrate RHA Shielding Material. The [100]- and [111]-oriented penetrators both produce relatively deep penetrations into RHA (Bruchey, Horwath, and Kingman 1991) with the [100] orientation being slightly better than the [111] orientation. Both of these directions have symmetrical deformation systems which provide an even mass transfer to the wall of the cavity. The difference lies in the [100] producing dislocations on slip planes and the [111] producing pure screw dislocations which don't have a slip or glide plane. Thus, the [100] orientation can work harden better than the [111] direction because its dislocations can react, impinge, or form barriers (i.e., become entangled) on slip planes, whereas the screw dislocations in the [111]-oriented penetrator are lines $\underline{b} = \underline{u}$ and thus have a reduced strain field which reduces their interaction.

The [110]-oriented penetrator does not have symmetrical deformation, which results in the penetrator becoming skewed in its track. Because skewing of the penetrator increases the area along the penetration axis, mushrooming of the head occurs (i.e., the diameter of the cavity hole increases, which decreases its total penetration depth. As well, because the [110]-oriented penetrator does not have symmetrical deformation in all directions and slip on the $[1\bar{1}0]$ (as well as, possibly, deformation by screw dislocations which twist the penetrators' head around to the $[111][1\bar{1}0]$) mass transfer for the [110] penetrator occurs somewhat easier than the [100]- and [111]-oriented penetrators (i.e., the [110] penetrator has only a few active slip systems operative and thus does not work harden as much as the [100] and [111] penetrators). The dislocations flowing along the $(1\bar{1}0)$ experience very little resistance to glide since there would not be as many dislocations (relatively) on active slip planes which would try to pass through the $(1\bar{1}0)$ plane.

5. REFERENCES

Bruchey, W. J., E. J. Horwath, W. R. Rowe. "The Effect of Crystallographic Orientation on the Performance of Single Crystal Tungsten Sub-Scale Penetrators." Technical Report, U.S. Army Ballistic Research Laboratory, Aberdeen Proving Ground, MD, in publication.

Bruchey, W. J., E. J. Horwath, and P. W. Kingman. "Orientation Dependence of Deformation and Penetration Behavior of Tungsten Single-Crystal Rods." 1991 TMS Annual Meeting, Session on Tungsten and Tungsten Alloys: Recent Advances, New Orleans, LA, 17–21 February 1991.

Cottrel, A. H. Dislocations and Plastic Flow in Crystals. Oxford University Press, 1953.

Gerlach, U. "Microstructural Analysis of Residual Projectiles—A New Method to Explain Penetration Mechanisms." Metallurgical Transactions, Vol. 17A, p. 435, 1986.

Magness, L. S, and T. G. Farrand. "Deformation Behavior and Its Relationship to the Penetration Performance of High-Density KE Penetrator Materials." 1990 Army Science Conference. Durham, NC, 12–15 June 1990.

Rose, R. M., D. P. Ferriss, and J. Wulff. "Yielding and Plastic Flow in Single Crystals of Tungsten." Transactions of the Metallurgical Society of AIME, Vol. 224, p. 981, 1962.

Stephens, J. R. "Dislocation Structures in Slightly Strained Tungsten, Tungsten-Rhenium, and Tungsten-Tantalum Alloys." *Transactions of the Metallurgical Society of AIME*, Vol. 242, p. 634, 1968.

Taylor, J. L. "Slip in Tungsten at High Temperatures." NASA Technical Report No. 32–818, p. 9, 1965.

Weertman, J., and J. R. Weertman. Elementary Dislocation Theory. MacMillan Series in Material Science, 1965.

INTENTIONALLY LEFT BLANK.

No. of Copies	Organization
2	Administrator Defense Technical Info Center ATTN: DTIC-DDA Cameron Station Alexandria, VA 22304-6145
1	Commander U.S. Army Materiel Command ATTN: AMCAM 5001 Eisenhower Ave. Alexandria, VA 22333-0001
1	Commander U.S. Army Laboratory Command ATTN: AMSLC-DL 2800 Powder Mill Rd. Adelphi, MD 20783-1145
2	Commander U.S. Army Armament Research, Development, and Engineering Center ATTN: SMCAR-IMI-I Picatinny Arsenal, NJ 07806-5000
2	Commander U.S. Army Armament Research, Development, and Engineering Center ATTN: SMCAR-TDC Picatinny Arsenal, NJ 07806-5000
1	Director Benet Weapons Laboratory U.S. Army Armament Research, Development, and Engineering Center ATTN: SMCAR-CCB-TL Watervliet, NY 12189-4050
(Unclass. only)1	Commander U.S. Army Rock Island Arsenal ATTN: SMCRI-TL/Technical Library Rock Island, IL 61299-5000
1	Director U.S. Army Aviation Research and Technology Activity ATTN: SAVRT-R (Library) M/S 219-3 Ames Research Center Moffett Field, CA 94035-1000
1	Commander U.S. Army Missile Command ATTN: AMSMI-RD-CS-R (DOC) Redstone Arsenal, AL 35898-5010

No. of Copies	Organization
1	Commander U.S. Army Tank-Automotive Command ATTN: ASQNC-TAC-DIT (Technical Information Center) Warren, MI 48397-5000
1	Director U.S. Army TRADOC Analysis Command ATTN: ATRC-WSR White Sands Missile Range, NM 88002-5502
1	Commandant U.S. Army Field Artillery School ATTN: ATSF-CSI Ft. Sill, OK 73503-5000
(Class. only)1	Commandant U.S. Army Infantry School ATTN: ATSH-CD (Security Mgr.) Fort Benning, GA 31905-5660
(Unclass. only)1	Commandant U.S. Army Infantry School ATTN: ATSH-CD-CSO-OR Fort Benning, GA 31905-5660
1	WL/MNOI Eglin AFB, FL 32542-5000
	Aberdeen Proving Ground
2	Dir, USAMSAA ATTN: AMXSY-D AMXSY-MP, H. Cohen
1	Cdr, USATECOM ATTN: AMSTE-TC
3	Cdr, CRDEC, AMCCOM ATTN: SMCCR-RSP-A SMCCR-MU SMCCR-MSI
1	Dir, VLAMO ATTN: AMSLC-VL-D
10	Dir, USABRL ATTN: SLCBR-DD-T

No. of
Copies Organization

2 Commander
U.S. Army Armament Research,
Development, and Engineering Center
ATTN: SMCAR-AET-M,
Bill Tanner
Deepak Kapoor
Picatinny Arsenal, NJ 07806-5000

1 Director
U.S. Army Materials Technology Laboratory
ATTN: SLCMT-MEM, Ken Tauer
Watertown, MA 02172-0001

2 Director
Los Alamos National Laboratory
ATTN: Anthony D. Roller, Mail Stop G-700
Bill Hogan, Mail Stop F-681
P.O. Box 1663
Los Alamos, NM 87545

2 University of California, San Diego
Department of Applied Mechanics and
Engineering Sciences, B-010
ATTN: Prof. Kenneth Vechhio
Prof. Marc Meyer
La Jolla, CA 92093

1 Johns Hopkins University
ATTN: Prof. Bob Green
Maryland Hall
34th & Charles Street
Baltimore, MD 21218

1 Johns Hopkins Univeristy
ATTN: Dr. Ramesh
Latrobe 104
34th & Charles Street
Baltimore, MD 21218

1 Adleman Assoc.
ATTN: Carl Cline
3301 El Amino Rial, Suite 280
Atherta, CA 94027

1 Failure Analysis Associates
Engineering & Scientific Services
ATTN: Mr. Stephen Andrews
P.O. Box 3015
149 Commonwealth Drive
Menlo Park, CA 94025

USER EVALUATION SHEET/CHANGE OF ADDRESS

This Laboratory undertakes a continuing effort to improve the quality of the reports it publishes. Your comments/answers to the items/questions below will aid us in our efforts.

1. BRL Report Number BRL-TR-3385 Date of Report August 1992

2. Date Report Received _____

3. Does this report satisfy a need? (Comment on purpose, related project, or other area of interest for which the report will be used.) _____

4. Specifically, how is the report being used? (Information source, design data, procedure, source of ideas, etc.) _____

5. Has the information in this report led to any quantitative savings as far as man-hours or dollars saved, operating costs avoided, or efficiencies achieved, etc? If so, please elaborate. _____

6. General Comments. What do you think should be changed to improve future reports? (Indicate changes to organization, technical content, format, etc.) _____

CURRENT ADDRESS

Name

Organization

Address

City, State, Zip Code

7. If indicating a Change of Address or Address Correction, please provide the New or Correct Address in Block 6 above and the Old or Incorrect address below.

OLD ADDRESS

Name

Organization

Address

City, State, Zip Code

(Remove this sheet, fold as indicated, staple or tape closed, and mail.)

DEPARTMENT OF THE ARMY
Director
U.S. Army Ballistic Research Laboratory
ATTN: SLCBR-DD-T
Aberdeen Proving Ground, MD 21005-5066

OFFICIAL BUSINESS

BUSINESS REPLY MAIL
FIRST CLASS PERMIT No 0001, APG, MD

Postage will be paid by addressee.

Director
U.S. Army Ballistic Research Laboratory
ATTN: SLCBR-DD-T
Aberdeen Proving Ground, MD 21005-5066

NO POSTAGE
NECESSARY
IF MAILED
IN THE
UNITED STATES

END

FILMED

DATE: 10-92

DTIC